Arabian Journal of Chemistry (2022) **15**, 103745

King Saud University

Arabian Journal of Chemistry

www.ksu.edu.sa
www.sciencedirect.com

ORIGINAL ARTICLE

$CoFe_2O_4$@Methylcellulose/AC as a New, Green, and Eco-friendly Nano-magnetic adsorbent for removal of Reactive Red 198 from aqueous solution

Alireza Nasiri [a,b], **Saeed Rajabi** [c,d], **Majid Hashemi** [e,*]

[a] *Environmental Health Engineering Research Center, Kerman University of Medical Sciences, Kerman, Iran*
[b] *Department of Environmental Health Engineering, Faculty of Public Health, Kerman University of Medical Sciences, Kerman, Iran*
[c] *Department of Environmental Health Engineering, School of Health, Shiraz University of Medical Sciences, Shiraz, Iran*
[d] *Student research committee, Shiraz University of Medical Sciences, Shiraz, Iran*
[e] *Student Research Committee, Kerman University of Medical Sciences, Kerman, Iran*

Received 6 December 2021; accepted 25 January 2022
Available online 01 February 2022

KEYWORDS

Nano-Magnetic Adsorbent;
Multifactorial Mesoporous;
Water Treatment;
Dye

Abstract Methylcellulose (MC) is the most common commercial cellulose ether and the most attractive biopolymer due to its cheap cost of biodegradability, biocompatibility, hydrophilicity, and lack of toxicity. In this study, $CoFe_2O_4$@MC/activated carbon (AC) was synthesized as a unique magnetic nano-adsorbent in the presence of MC biopolymer for Reactive Red 198 (RR198) dye removal. The nano-magnetic adsorbent was characterized by FESEM (Field emission scanning electron microscopy), EDS (Energy-dispersive X-ray spectroscopy), Mapping, Linescan, BET (Brunauer–Emmett–Teller), FTIR (Fourier Transform Infrared Spectroscopy), XRD (X-Ray Diffraction), and VSM (Vibrating-Sample magnetometer). For simple separation by external magnetic fields, the Ms value was 57.91 emu/g. According to XRD analysis, the nano-adsorbent maintains its crystal structure, with an average crystal size of 11 nm. The maximum removal efficiencies of RR198 for synthetic and real wastewater samples under optimal conditions (an initial concentration of 10 mg/L, pH 3, contact time of 10 min, nanocomposite dose of 1.5 g/L, and a temperature of 25 °C) were 92.2% and 78%, respectively. The adsorption experiments were fitted well with the Freundlich isotherm (R^2 = 0.989) and *pseudo*-second-order kinetic (R^2 = 0.995). The values of entropy changes (ΔS = 35.087 kJ/mol.k), enthalpy changes (ΔH = -9.862 kJ/mol), and negative Gibbs free energy changes (ΔG) showed that the adsorption process was exothermic. Finally,

* Corresponding author at: Student Research Committee, Kerman University of Medical Sciences, Kerman, Iran.
E-mail address: mhashemi120@gmail.com (M. Hashemi).
Peer review under responsibility of King Saud University.

Production and hosting by Elsevier

https://doi.org/10.1016/j.arabjc.2022.103745

the reusability findings showed that after six recovery cycles, the efficiency decreased slightly (90.1%). In the end, it can be concluded that the prepared $CoFe_2O_4$@Methylcellulose/AC can be used as an efficient adsorbent for the removal of RR198 from an aqueous solution.

1. Introduction

Given that water is considered to be the most vital factor for life and survival on Earth, this justifies the need for healthy and pollution-free water resources (Aichour et al., 2022, Sobhanardakani et al., 2013). The growth of societies towards industrialization and modernity has caused serious problems in providing safe water (Zandipak and Sobhanardakani, 2016). One of the most important and serious problems is the presence of different concentrations of pollutants such as insecticides, antibiotics, dyes, and chemical fertilizers (Nasiri et al., 2019a, Iervolino et al., 2019, Javid et al., 2019, Sobhanardakani and Zandipak, 2015).

Synthetic dyes are compounds that are widely used in textile, cosmetics, leather, paper, and similar industries (Sanjid Qais et al., 2021, Salimi et al., 2017). Since the industries that produce these dyes, discharge the wastewater containing these dyes into rivers, lakes, and other water sources, they cause serious problems due to their high toxicity and accumulative nature in the environment (Mahdizadeh et al., 2020, Malakootian et al., 2020a, Zandi Pak and Sobhan Ardakani, 2016, Sobhanardakani et al., 2016). These dyes are divided into Reactive, Azo, Acid, Basic, Direct, and dispersing categories based on their chemical structure and methods of use. Most of these dye contaminants originate from the textile industry (Kausar et al., 2018, Malakootian et al., 2019b, Salimi et al., 2019a). Reactive Red 198 dye (RR198) is one of the dyes used in this study.

RR198 is an anionic dye from the group of Azo dyes with molecular formula $C_{27}H_{18}C_1N_7Na_4O_{15}S_5$ and heterocyclic, which has a multi-ring structure and mono-Azo (-N = N-) (Dehghani et al., 2018). Azo dyes can remain in the environment for a long time due to their high stability. The presence of these dyes in water threatens the life of aquatic plants and animals and leads to a decrease in photosynthesis (Afolabi et al., 2021, Rashad et al., 2017b). Most of these dyes are carcinogenic and mutagenic in animals (Unnikrishnan et al., 2018, Nasiri et al., 2021b, Mahmoud et al., 2012). The effects of these dyes on humans include allergies, dermatitis, skin irritation, carcinogenesis, and genetic mutations (Sadeghi et al., 2018, Malakootian et al., 2020c, Sobhanardakani et al., 2017). To reduce hazards and adverse effects of these dyes on the environment, effluents containing these materials must be treated by appropriate methods (Baghapour et al., 2014, Carneiro et al., 2010, Sanad et al., 2021b, Rashad et al., 2017a).

There are various methods and technologies for the treatment of these polluted waters that are used with the three purposes of reducing water resources, water treatment, and recycling (Malakootian et al., 2019c, Malakootian et al., 2019a, Das et al., 2020a, Das et al., 2021, Das et al., 2020b). Despite these different methods and technologies for water treatment, there are still issues of economic efficiency, high efficiency, and speed of treatment that must be considered. Methods and technologies used in water treatment include distillation, evaporation, oxidation, ion exchange, reverse osmosis, electrolysis, crystallization, solvent extraction, precipitation, filtration, adsorption, electrodialysis (Chavoshani et al., 2018, Fadaei et al., 2017, Mohammadi et al., 2019, Das and Debnath, 2021, Rashad et al., 2017a). Each of these methods has disadvantages, the most important of which are high cost, high energy consumption, low speed, production of secondary pollutants and sludge, low efficiency, etc. (Gupta et al., 2012, Hashemi et al., 2017, Nasiri et al., 2019b, Debnath et al., 2020).

Compared to other water treatment methods, the adsorption method is used due to relatively low operation costs, high process efficiency, no need for regular system monitoring, low energy consumption, and no sludge production (Malakootian et al., 2018a, Salimi et al., 2019b, Debnath et al., 2017, Bhowmik et al., 2019). In this treatment method, various adsorbents are used, some of which are naturally available and some of which are synthetical available. Adsorption methods use adsorbents from the surface and biological groups. Surface adsorbents include activated carbon, single-walled and multi-walled carbon nanotubes, and graphene oxide, but their use is restricted due to a high time- and cost separation from reaction medium (Pourzamani et al., 2018, Pourzamani et al., 2017, Sadeghi et al., 2018). Some of these adsorbents are not easily separated despite having a high surface area (Malakootian et al., 2020b). Time-consuming methods such as filtration and centrifugation are required for the separation of adsorbents from the process environment (Pourzamani et al., 2017, Pourzamani et al., 2018).

For easy and fast separation of adsorption from the process environment and providing the possibility of recovery and reuse of these adsorbents, the problem of separation and reuse can be solved by magnetizing these compounds (Malakootian et al., 2015, Crini, 2006). Nanoparticles like iron oxides are used to get around these limitations. In recent years, a novel form of magnetic adsorbent has been created by combining metals like iron and cobalt with inorganic materials. These magnetic nanoparticles offer several benefits, including ease of separation using an external magnetic field, inexpensive manufacturing costs, ability to regenerate, and a high adsorption capacity (Mehdinejad et al., 2018, Rajabi et al., 2022, Mohammadi et al., 2019).

So far, various magnetic nano adsorbents such as $CoFe_2O_4$/Graphene oxide for adsorption organic pollutants (Chang et al., 2020), SiO_2@$CoFe_2O_4$/GO for adsorption anionic pollutants (Santhosh et al., 2017), $CoFe_2O_4$/AC for adsorption Cr(VI) (Qiu et al., 2016), $CoFe_2O_4$/vacancy@ $mSiO_2$ for adsorption organic pollutants (Lu et al., 2019), $CuFe_2O_4$/Activated Carbon (Zhang et al., 2011), $CoFe_2O_4$/Co_xFe_x/AC for adsorption methylene blue (Xu et al., 2014), Chitosan/SiO_2/Fe_3O_4/AC for adsorption Cu^{2+} (Li et al., 2017), $CoFe_2O_4$-

Chitosan-Graphene (Zhang et al., 2014), MWCNT/$CoFe_2O_4$-NH_2 for adsorption mercury ions (Zhou et al., 2014) and $CoFe_2O_4$-TETA-GO for adsorption Cr(VI) (Sun et al., 2016) are synthesized and used as adsorbent.

To create novel biomaterials with innovative physicochemical characteristics, contaminants have been removed from water and wastewater, chemically modified polysaccharides widely explored. To reduce treatment costs while preventing the formation of harmful by-products at the end of the process, eco-friendly adsorbents (polysaccharides) must be used (Crini, 2005). Polysaccharides also have remarkable features such as particular structure, good chemical stability, strong reactivity, affinity, and selectivity for dyes and aromatic compounds due to the presence of various functional groups on their surface such as hydroxyl, amino, or acetamido (Mittal et al., 2016).

The most prevalent polysaccharide found in nature is cellulose, a regular and linear polymer consisting of (1 → 4) units of β-d-glucopyranosyl linked together. This β-(1 → 4) arrangement, when combined with intramolecular hydrogen bonding, results in a stiff structure. Intramolecular hydrogen bonding forming between hydroxyl groups is a result of aggregates or crystalline form. This connection between the single molecules is attributed to cellulose's water insolubility, resulting in the creation of highly organized crystalline areas (Moon et al., 2011). This morphology is associated with and regulates the source of cellulose, with the consequential limited accessibility to reactants. The cellulose ether, for example, methylcellulose (MC), hydroxypropyl-methylcellulose (HPMC), hydroxyethylcellulose (HEC), and carboxymethylcellulose (CMC), are important categories of modified polymers (Heinze and Koschella, 2005). The distribution of substituents throughout the cellulose backbone is typically uneven in derivatives produced under diverse circumstances.

MC is one of the most widely used commercial cellulose ethers, with uses in a wide range of industries. The hydroxyls at C-2, C-3, and/or C-6 positions of anhydrous-d-glucose units are replaced by methyl groups (–CH_3) in MC. This cellulose derivative exhibits unique physicochemical characteristics as well as amphiphilic qualities. Because of its bio-renewable, biocompatible, and biodegradable characteristics, MC is the most frequent and abundant green biopolymer, with many applications for humans (Rogers and Wallick, 2012).

Heavy metal ions, dyes, oil, pesticides, and radioactive metals are just a few of the harmful pollutants that may be removed from water and wastewater solutions using cellulose-based adsorbents (Crini, 2005). Traditional cellulose-based adsorbents' low adsorption capacity and separation issues limit their usage. To address these issues, magnetic adsorbents made from cellulose derivatives have been proposed as a suitable material for removing contaminants from water and wastewater (Sun et al., 2014). These chemicals feature functional groups that enhance the contact between the contaminant and the adsorbent surface, such as amino, hydroxyl, and carboxylic. Because of their chemical diversity, these chemicals can improve the physicochemical characteristics of magnetic nanoparticles (Tamaddon et al., 2020).

In this work, $CoFe_2O_4$@MC/AC was synthesized for the first time in the presence of MC biopolymer as a new magnetic nano-adsorbent for RR198 dye removal. The advantages of this magnetic nano-adsorbent include fast and high-efficiency synthesis, synthesis in the presence of MC as a biopolymer, no use of harmful chemical compounds, and no use of surfactants. Adsorption isotherms, kinetics, and thermodynamics were examined while optimizing process parameters such as solution pH, initial concentration, adsorbent dosage, and contact time. Reusability and chemical stability of nano-biocomposite were also assessed.

2. Materials and methods

2.1. Chemicals and instrumentation

All chemicals and reagents including iron (III) chloride hexahydrate ($FeCl_3{\cdot}6H_2O$), Cobalt (II) chloride hexahydrate ($CoCl_2{\cdot}6H_2O$), Methylcellulose (MC), Sodium hydroxide (NaOH), and Activated carbon (AC) were purchased from Sigma Aldrich Company (United States). Reactive red 198 (RR198) was purchased from Alvan Paint Company (Tehran, Iran). Deionized water was used during the experiments. HCl and NaOH were used for adjusting the solution pH. In this study, devices such as spectrophotometer (SHIMADZU, UV-1800), microwave (SAMSUNG, 2450 MHz, 800 W), and pH meters (HANNA instruments, pH 212) were used.

2.2. Preparation of $CoFe_2O_4$@MC/AC

In 100 mL of distilled water (DW), $FeCl_3{\cdot}6H_2O$ (5.4 g) and $CoCl_2{\cdot}6H_2O$ (2.38 g) (in a molar ratio of 2:1) were dissolved, followed by 1 g of MC. Then NaOH was added for 1 h. to alkalize the pH of the solution (Nasiri et al., 2021a, Nasiri et al., 2019c, Nasiri et al., 2019d, Rajabi et al., 2022). Then, 1 g of activated carbon was added to the reaction container and stirred. After adding activated carbon to the solution, to complete the reaction the mixture was placed in the microwave at 450 W for 15 min (3 × 5 min) to obtain a black precipitate. The obtained precipitate as a product was separated using a magnet and washed several times with deionized water to neutralize the final pH. Finally, the black precipitate was dried for 24 h at 70 °C temperature in the oven (Fig. 1).

2.3. Instrument details

This black precipitate, which acts as a magnetic nano adsorbent, was structurally characterized by XRD to identify the crystal structure and phase of the magnetic nano-adsorbent (PHILIPS PW1730), FTIR to study chemical bonds and determine functional groups in magnetic nano-adsorbent (AVATAR, Thermo), FESEM to study the shape, content, and surface structure of magnetic nano-adsorbent at nanoscale dimensions (TESCAN MIRA III), EDS-Mapping & Linescan to study the weight percentage of elements, type of elements and distribution of elements at the surface of magnetic nano-adsorbent (TESCAN MIRA II, SAMX Detector), BET to measure the specific area of a magnetic nano-adsorbent (BELSORP MINI II) and VSM to measure the magnetic behavior of magnetic nano-adsorbent (LBKFB, Kashan Kavir Magnet Company) devices. After confirming the physical and chemical structure of the magnetic nano adsorbent, this compound was used as an adsorbent in the Reactive Red 198 (RR198) dye removal process.

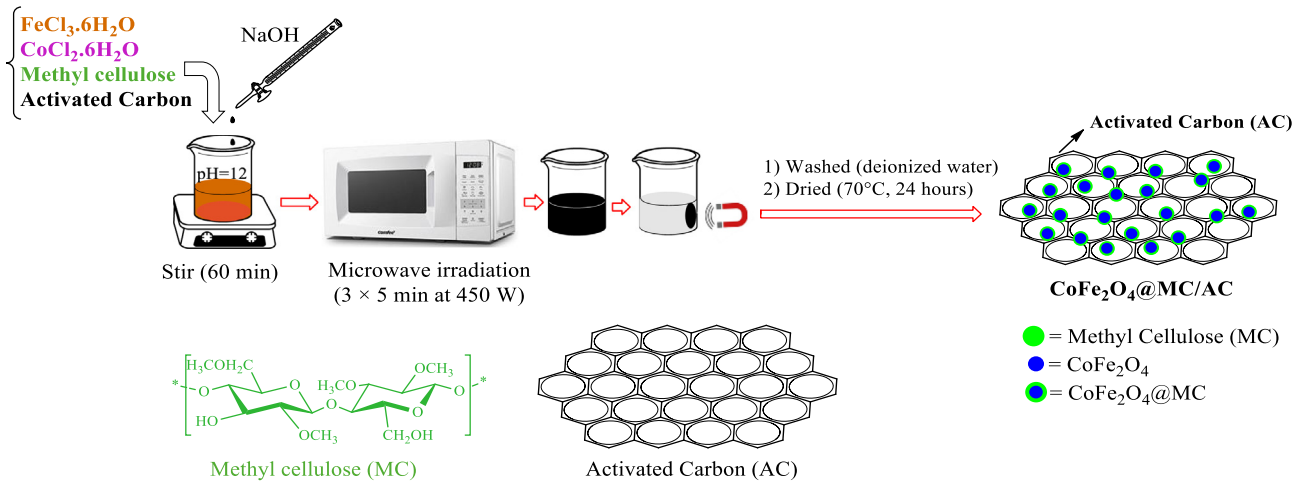

Fig. 1 Schematic of $CoFe_2O_4$@MC/AC preparation.

2.4. Batch adsorption experiments

At first, the RR198 dye stock solution was made with a concentration of 500 mg/L and then concentrations of 10, 15, 20, 30, and 40 mg/L were prepared from it. To optimize the adsorbent dose, amounts of 0.25, 0.5, 1, 1.5, and 2 g/L were investigated. Solutions of 1 *N* NaOH and HCl were used to adjust the pH and pHs of 3, 5, 7, 9, and 11 were surveyed. Contact times of 2, 5, 10, 15, and 20 min and temperatures of 25, 30, 35, and 40 °C were investigated and optimized. A real wastewater sample was taken from the Kerman University of Medical Sciences campus in Iran to assess the RR198 adsorption effectiveness of the $CoFe_2O_4$@MC/AC magnetic nanoadsorbent, the physiochemical properties of which were measured when a given amount of RR198 was added. The rate of RR198 adsorption performance by $CoFe_2O_4$@MC/AC magnetic nanocomposite was reported after experiments were conducted on wastewater under ideal conditions.

Finally, the adsorption efficiency (Eq. (1)) and adsorption capacity (Eq. (2)) were calculated by the following formulas:

$$R_e(\%) = \frac{C_0 - C_t}{C_0} \times 100 \quad (1)$$

R_e is adsorption efficiency (%), C_0 and C_t are initial concentration and final concentration (mg/L), respectively (Nasseh et al., 2019).

$$Q_v = \frac{(C_0 - C_t)V}{m} \quad (2)$$

Q_e is adsorption capacity, C_0 and C_t are initial concentration and final concentration (mg/L), respectively. V is the volume of solution (L), m is adsorption mass (g) (Nasseh et al., 2019).

2.5. Determine of pH_{zpc}

By using the solid addition technique, the pH zero point of charge (pH_{zpc}) of $CoFe_2O_4$@MC/AC was found. At 6 various pH (2–12) values, 100 mL of KCl solution (0.1 M) was produced. Each solution received 0.01 g of magnetic nano adsorbent. For 24 h, the produced combinations were stored at room temperature. A pH meter was used to determine the initial and final pH of the solutions. The pH_{zpc} was calculated by plotting the $\Delta pH = pH_f - pH_i$ equation and the pH_i. The pH_{zpc} was chosen as the crossing point of ΔpH = zero. The solutions of NaOH and HCL (0.1 *N*) were used to alter the pH of the solutions (Datta et al., 2017, Malakootian et al., 2018b).

3. Results and discussion

3.1. Characterization of the synthesized magnetic nano adsorbent

Initially, the novel magnetic nano adsorbent $CoFe_2O_4$@MC/AC was prepared from Co^{2+} and Fe^{3+} with the existence of MC and AC by using a new microwave-assisted technique based on the experimental procedure. To characterize this magnetic nano-adsorbent, several techniques were applied.

The FESEM analysis of the synthesized $CoFe_2O_4$@MC/AC was used to determine the form and size. FESEM pictures of $CoFe_2O_4$@MC/AC synthesized in the existence of methylcellulose as a biopolymer are shown in Fig. 2a-d. In the composite structure, the influence of methylcellulose on the morphological of $CoFe_2O_4$@MC/AC resulted in a smooth, homogeneous, and poorly aggregated sphere-shaped magnetic nano adsorbent (11 nm). EDS analysis was used to assess the purity and chemical content of the produced $CoFe_2O_4$@MC/AC (Fig. 2e) The chemical structure of $CoFe_2O_4$@MC/AC magnetic nano-adsorbent shows 34.71% Fe, 32.21% O, 19.18% Co, and 13.89% C, which are all within the predicted range. The distribution of $CoFe_2O_4$@MC/AC magnetic nano-adsorbent elements was investigated using Mapping and Line scanning. According to the data shown in Fig. 2f, Co, Fe, O, and C exhibited a homogenous distribution, indicating that the synthesized $CoFe_2O_4$@MC/AC had a high homogeneity. Line scanning, as shown in Fig. 2 g, has further validated these findings.

Fourier transform infrared spectroscopy (FTIR) has been used to obtain the functional group of synthesized nanoparticles. By using a KBr disc, the powdered $CoFe_2O_4$@MC/AC was investigated (Fig. 3).

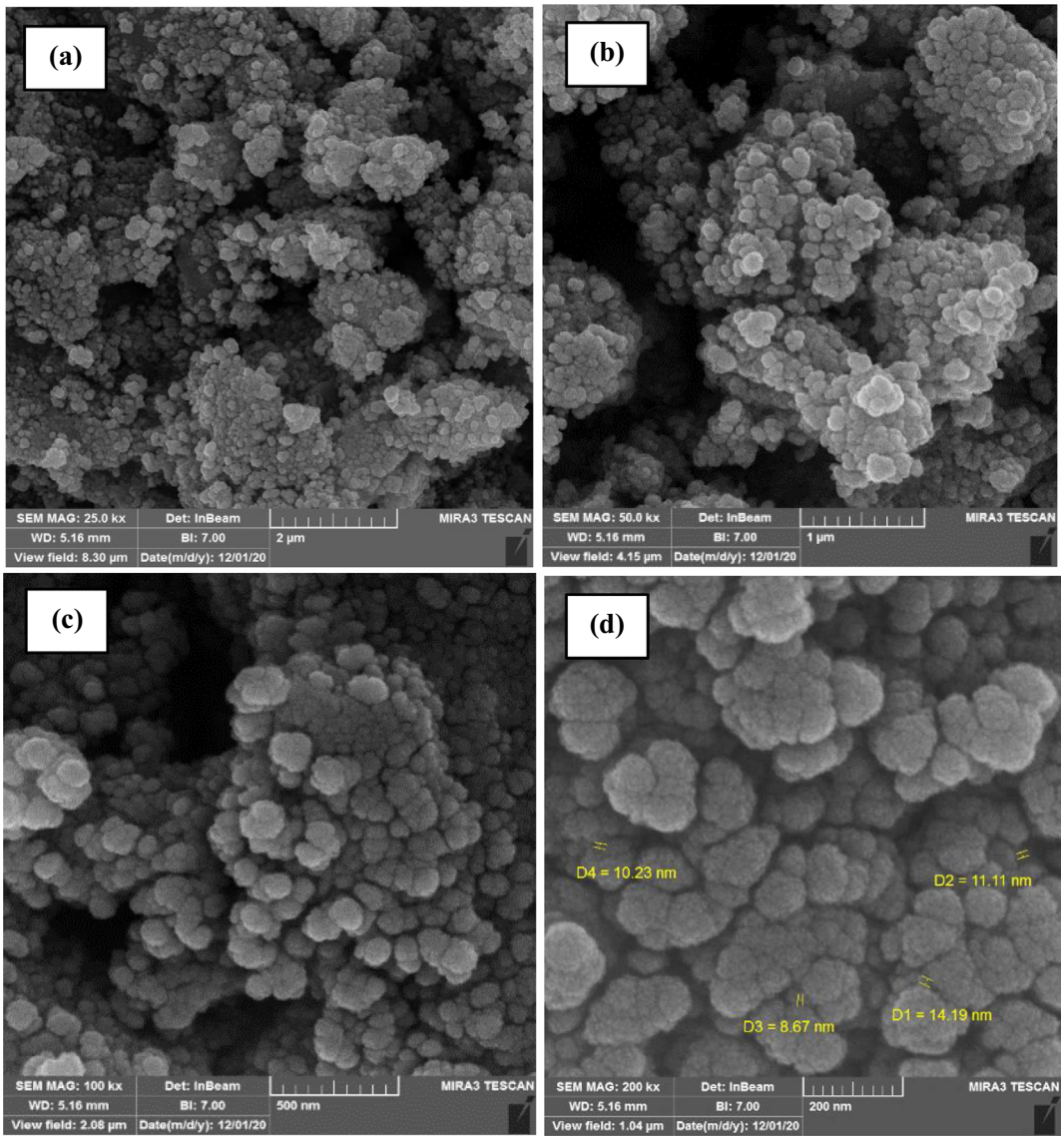

Fig. 2 FESEM images in 2 µm (a), 1 µm (b), 200 nm (c), 100 nm (d) resolutions, EDS (e), Mapping (f) and line scanning (g) of $CoFe_2O_4$@MC/AC magnetic nano-adsorbent.

The absorption peaks of MC at 3461, 2931, 1644, 1457, 1377–1315, 1066, and 946 cm^{-1} are associated with O-H stretching, C-H stretching, adsorbed water stretching, methylene group C-H bending, methyl group C-H bending, C-O stretching, and C-O-C stretching vibrations of the methylcellulose glycosidic bond, and = C-H bending, respectively, as shown in Fig. 3 (Liebeck et al., 2017, Fahad et al., 2017). Ion vibrations in the crystalline lattice are commonly measured in the 4000–400 cm^{-1} region (Brabers, 1969). The tetrahedral and octahedral structures of spinel ferrites are allocated to the upper-frequency band (ν_1 = 569 cm^{-1}) and frequencies lower band (ν_2 = 473 cm^{-1}) respectively (Modi et al., 2006). Inverse spinel ferrites are known for their high absorption bands (Pradeep et al., 2008).

XRD analysis was used to characterize structures, phases, and crystalline composition of $CoFe_2O_4$@MC/AC, and then the XRD spectra of methylcellulose and adsorbent are compared. The achieved results are shown in Fig. 4.

The XRD pattern of MC presents a prominent peak centered at 18.23°. Based on the JCPDS 96–591-0064, the $CoFe_2O_4$@MC/AC crystal phase structure and XRD pattern with diffraction peaks at 2θ = 29.98°, 35.31°, 42.95°, 53.47°, 56.82°, 62.47°, and 74.15° are indexed to the $CoFe_2O_4$ cubic spinel phase. According to the obtained results, the $CoFe_2O_4$ crystal structure was well protected in the MC and AC composition. It is so interesting, that the XRD spectrum of $CoFe_2O_4$@MC/AC indicates the characteristic peaks linked with both MC and AC and $CoFe_2O_4$, which points to the successful synthesis of $CoFe_2O_4$@MC/AC magnetic nano-adsorbent.

Fig. 5 shows adsorption/desorption isotherm, BET-BJH specific surface area, and t-plot of the synthesized $CoFe_2O_4$@MC/AC (Figs. 5a-d).

The specific surface area, average pore diameter, and total porosity volume (p/p_0 = 0.99) of the synthesized magnetic nano-adsorbent were 128.22 m^2/g, 7.1194 nm, and 0.2282 cm^3/g, respectively, according to the BET plot. Pores

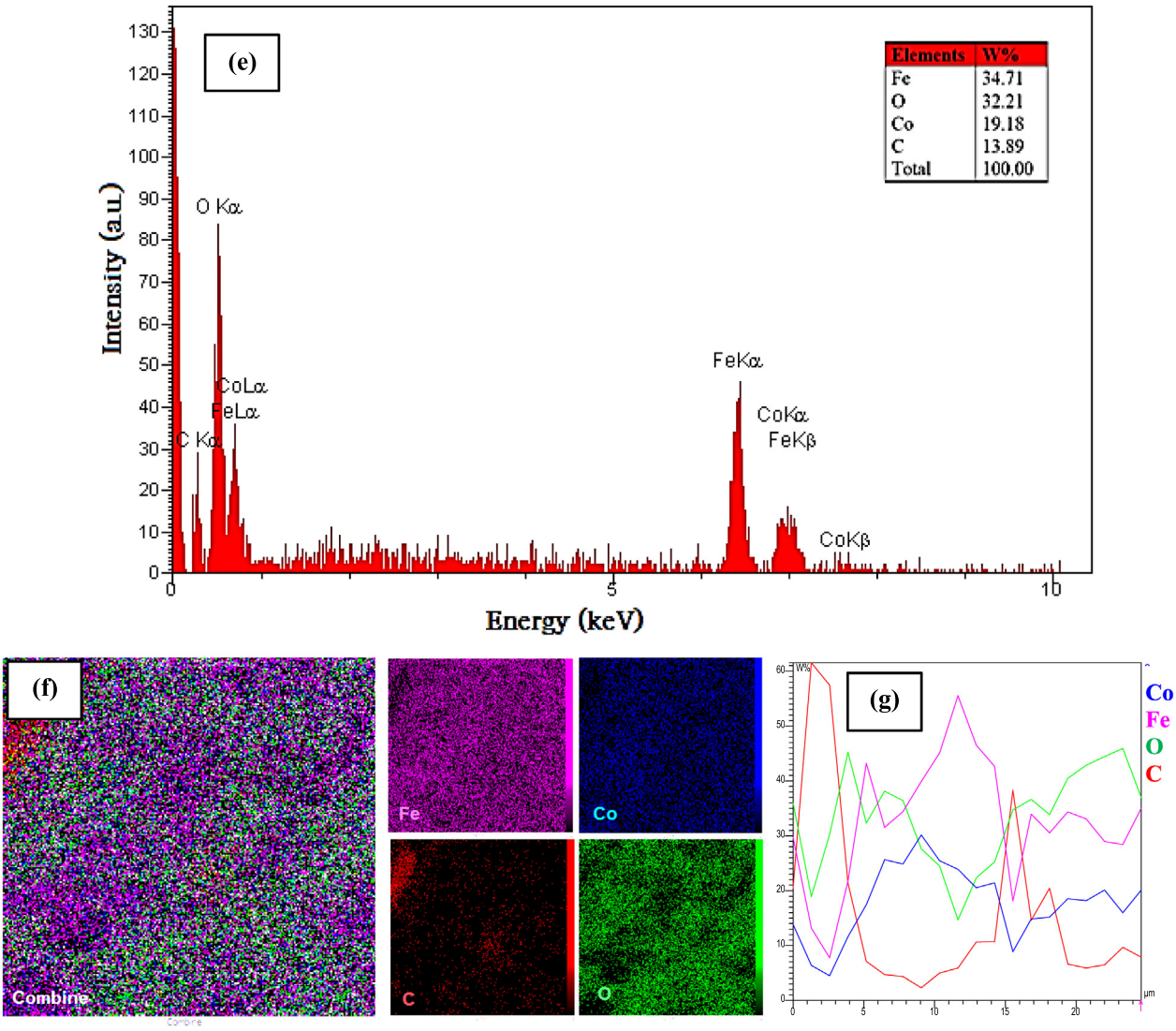

Fig. 2 (*continued*)

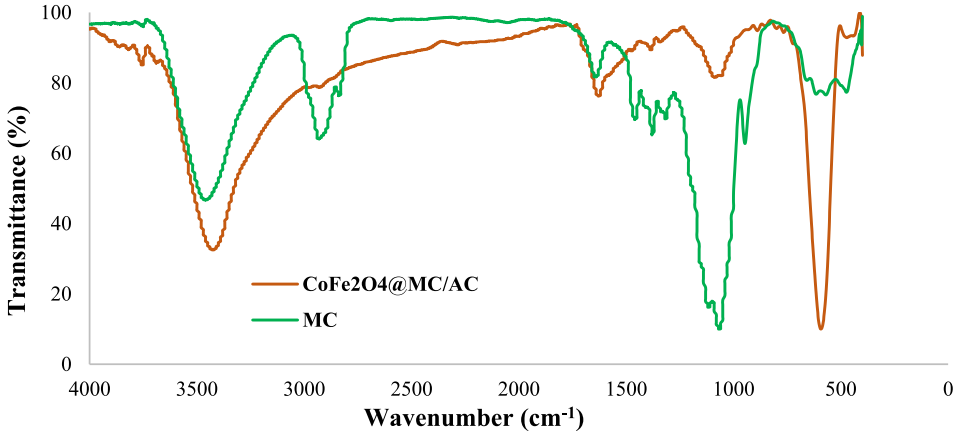

Fig. 3 FTIR of $CoFe_2O_4$@MC/AC magnetic nano-adsorbent and MC.

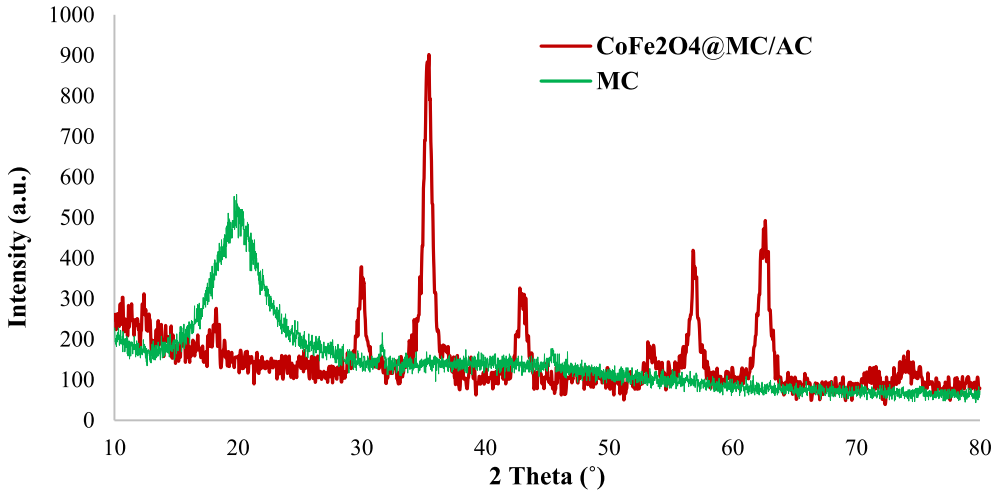

Fig. 4 The XRD patterns of $CoFe_2O_4$@MC/AC magnetic nano-adsorbent and MC.

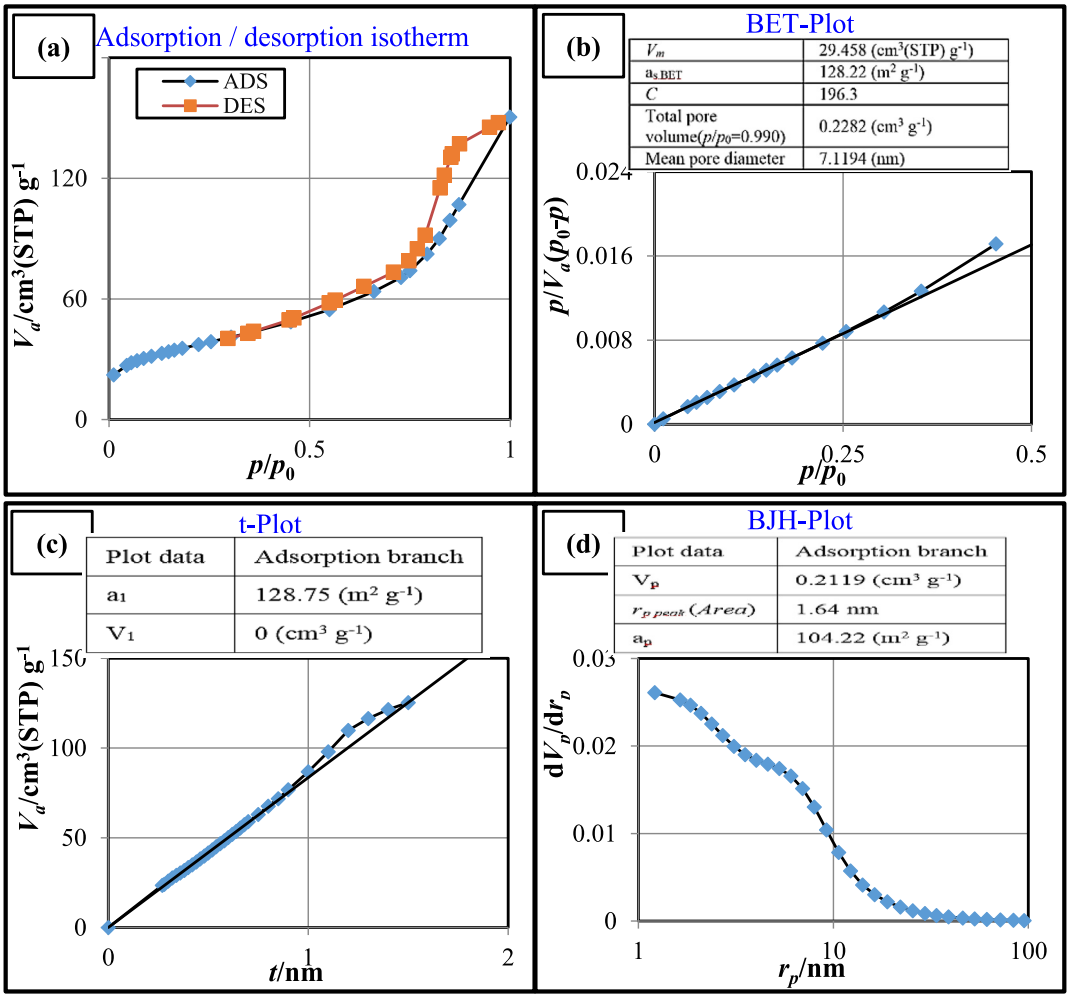

Fig. 5 Adsorption/desorption isotherm (a), BET surface area (b), t-Plot (c) and BJH surface area (d) of $CoFe_2O_4$@MC/AC magnetic nano-adsorbent.

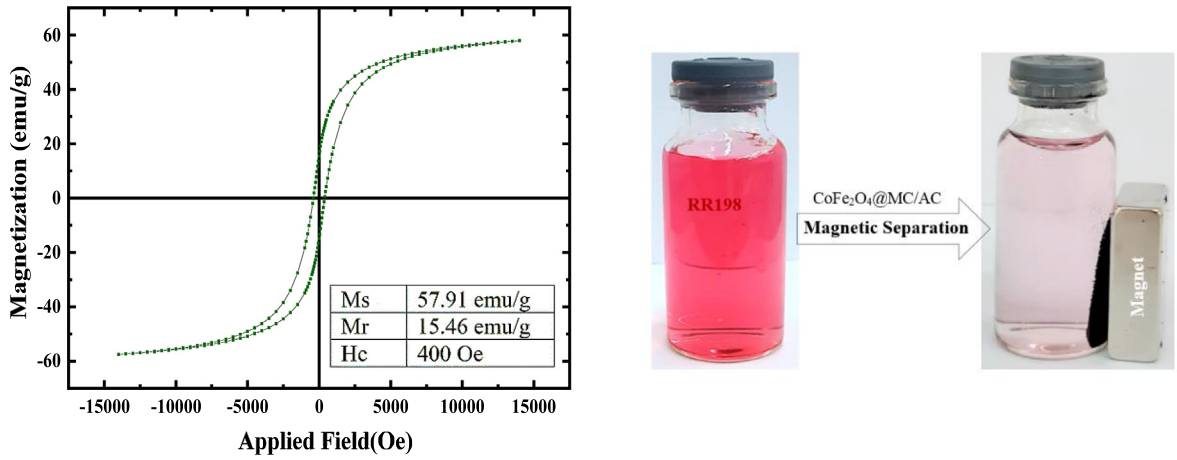

Fig. 6 VSM magnetization curve of $CoFe_2O_4$@MC/AC magnetic nano-adsorbent; the photo inset shows the solution after magnetic separation of the magnetic nano-adsorbent.

are divided into three categories by the IUPAC: microporous, mesoporous, and macroporous materials. According to the IUPAC description, a mesoporous material contains pores with dimensions ranging from 2 to 50 nm. Microporous pores are less than 2 nm and macroporous pores are greater than 50 nm, respectively. A mesoporous material, $CoFe_2O_4$@MC/AC, might be described. As depicted, the plots a Type-IV isotherm with a distinct hysteresis loop between the adsorption and desorption branches, indicating the existence of mesopores.

By using a vibrating sample magnetometer, The $CoFe_2O_4$@MC/AC magnetic nano-adsorbent property was examined (Fig. 6).

The measured values for residual magnetization (Mr), saturation magnetization (Ms), and coercive field (Hc) were 15.46 emu/g, 57.91 emu/g, and 400 Oe, respectively (Fig. 6). These results show the significant magnetic power of the $CoFe_2O_4$@MC/AC magnetic nano-adsorbent. The findings demonstrate that the magnetic characteristic of $CoFe_2O_4$ is retained in the $CoFe_2O_4$@MC/AC structure.

3.2. The influence of effective parameters on the adsorption process

3.2.1. Effect of adsorbent dose on RR198 adsorption

Adsorbent dosage is an important parameter in batch mode studies. The adsorbent dosage concentration from 0.25 to 2 g/L (0.25, 0.5, 1, 1.5, and 2) was studied on the removal of RR 198. As shown in Fig. 7 (a), the efficiency of dye removal was increased with the increase of adsorbent dose. Hence, the maximum dye adsorption was observed in 1.5 and 2 g/L doses of adsorbent that have maximum removal efficiency of 83.2% and 85.4% in 10 min, respectively in which the optimum dose of adsorbent is 1.5 g/L. The increasing of adsorbent dose cause to increase in the active sites and thus increases the available adsorption surface therefore, the adsorption rate will increase. Adding the further adsorbent may be caused to the saturation of the solution with the adsorbent resulting in, the active sites being out of reach and adsorption capacity decreasing (Santhosh et al., 2017, Alimohammadi et al., 2016). Liang et al. and Alimohammadi et al. conducted the same study on dye adsorption. They reported similar behavior for adsorption of Gentian violet and Reactive Red 198, respectively (Alimohammadi et al., 2016, Liang et al., 2019). Moussavi and Mahmoudi conducted the same study on the adsorption of Reactive Blue 19 and Reactive Red 198. They concluded that an increase in the adsorbent dose caused to increase in the removal efficiency and a further amount of adsorbent don't affect the high adsorption (Moussavi and Mahmoudi, 2009).

3.2.2. Effect of the initial concentration of RR198

In this study, dye concentration amounts of 10, 15, 20, 30, and 40 mg/L were studied. The effect of initial concentration on the removal of RR 198 was such that with increasing initial concentration from 10 to 40 mg/L, the removal efficiency decreased from 83.2% to 55.6% which is shown in Fig. 7 (b). The adsorption capacity of $CoFe_2O_4$@MC/AC increases quickly for the concentration of 10 mg/L in 5 min. Thus, the optimum initial concentration is 10 mg/L. This phenomenon occurs due to the saturation of the adsorption sites because a constant of adsorbent can only absorb a certain amount of the adsorbate. As a result, at low concentrations, the active sites are more and the rate of adsorption is higher (Gerard et al., 2016). The fastest removal rate was observed at this dye concentration which is due to the rapid diffusion of dye from the solution on the external surfaces of the adsorbent. After occupying the external sites, the adsorbed RR 198 tends to be transferred from the surface sites to inner sites, then in the same way, in the final stages of adsorption, the processing speed will be decreased (Liang et al., 2019). Liang et al. conducted the same study on the removal of gentian violet by $CoFe_2O_4$/Activated carbon. They concluded with increasing initial dye concentration; the removal efficiency was decreased (Liang et al., 2019). Torkian et al. also examined the adsorption of Congo Red onto mesoporous carbon that concluded the efficiency removal was decreased with increasing of the initial concentration of Congo Red (Torkian et al., 2012).

3.2.3. Effect of pH on RR198 adsorption

The pH is the most important parameter in charge of the surface of the adsorbent. In this study, pHs 3, 5, 7, 9, and 11 were investigated. As shown in Fig. 7 (c), the removal efficiency was

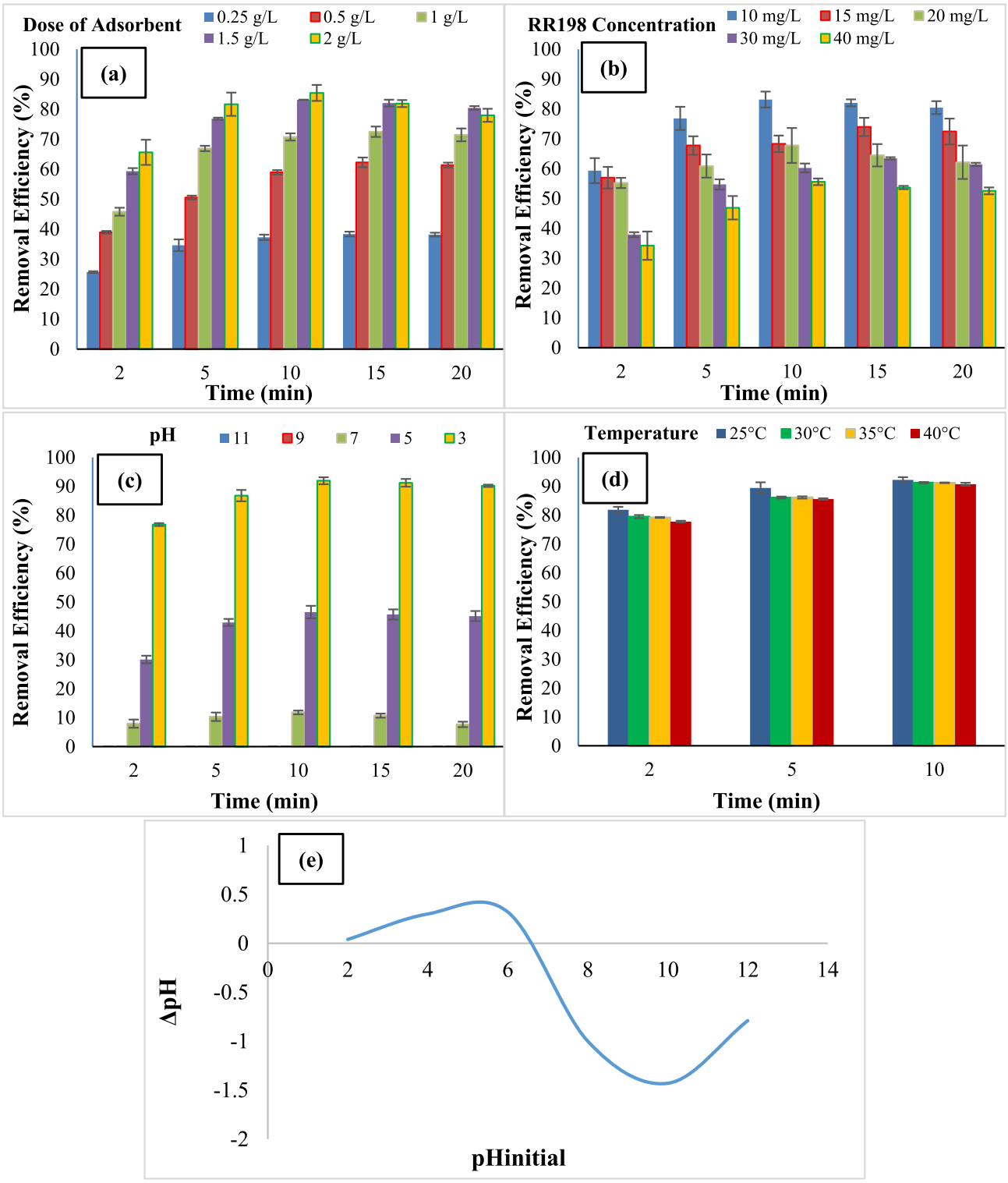

Fig. 7 Comparison of removal efficiency at a different adsorbent dose (a), RR198 initial concentration (b), pHs (c), temperatures (d), and pH_{zpc} (e) (Experimental conditions: RR198 concentration 10 mg/L, optimized pH 3, the dose of adsorbent 1.5 g/L).

increased with a decrease in the pH. In pHs 9 and 11, the removal efficiency was 0% but in pHs 7, 5, and 3, with decreasing pH from 7 to 3, the removal efficiency was increased from 12% to 92% in 10 min, thus optimum pH is 3. pH affects the adsorbent functional groups, the degree of the adsorbent molecules' ionization and the structure of the dye molecules. The Reactive Red 198 is an ionic dye that needs positive functional groups to be adsorption by the adsorbent. The surface of the adsorbent needs a positive charge, thus in the lower pH than pH_{zpc} = 6.6, the surface charge of the adsorbent

becomes positive, and the negatively charged groups of dye are attracted by the positively charged groups. Conversely, at high pHs, the adsorbent surface is charged with negative groups therefore, the adsorption of dye decreases (Fig. 7e) (Alimohammadi et al., 2016, Torkian et al., 2012). As a result, the electrostatic interactions play the main role in the adsorption of RR198 by adsorbent (Haffad et al., 2019). Alimohammadi et al. conducted the same study on adsorption of the Reactive Red 198 by walnut shells. They also concluded that the removal efficiency increases with decreasing pH (Alimohammadi et al., 2016). Ghaneian et al. and Haffad et al. also conducted the same work on the Reactive Red 198 removal by Pomegranate seed powder and chitosan, respectively. They concluded with decreasing pH, the removal efficiency increases (Haffad et al., 2019, Ghaneian et al., 2015).

3.2.4. Effect of temperature

The temperatures 25, 30, 35, and 40 °C were studied. As shown in Fig. 7 (d), with increasing temperature from 25 to 40 °C, the decolorization decreased slightly from 92.2% to 90.7%. as a result, the optimum temperature is 25 °C. Thus, dye adsorption by $CoFe_2O_4$@MC/AC is an exothermic process. When the temperature increase, the dye adsorption decreases, because the adsorption forces are being weaker and the bonding between adsorbent and adsorbate is reduced (de Farias Silva et al., 2020). Another hand, with increasing the temperature, the solubility of dye and also dissociation of dye increases as a result, the interaction between adsorbate and adsorbent decreases (Torkian et al., 2012). Kamranifar et al. and Torkian et al. conducted the same study on the removal of Reactive Red 195 and Congo Red, respectively. They reported the same behavior for the adsorption of these dyes with increasing temperatures (Torkian et al., 2012, Kamranifar et al., 2018).

3.2.5. Adsorption isotherm models

Isotherm is one of the most important parameters that should be studied in adsorption processes (Nasseh et al., 2019). In this study, three isotherms of Langmuir, Freundlich, and Temkin were investigated that were used to determination of adsorption capacity. The Langmuir isotherm is used for a homogeneous adsorbent surface for monolayer adsorption and the Freundlich isotherm is used for multilayer adsorption on the surface of heterogeneous adsorbent (Santhosh et al., 2017). The Langmuir isotherm (Eq. (3)) and Freundlich isotherm (Eq. (4)) were calculated by the following formulas and their curves were shown in Fig. 8.

$$\frac{C_e}{Q_e} = \frac{1}{Q_{max}K_L} + \frac{C_e}{Q_{max}} \tag{3}$$

$$lnQ_e = \left(\frac{1}{n}\right) lnC_e + lnK_f \tag{4}$$

C_e is RR198 concentration of equilibrium in the solid phase (mg/g), Q_{max} is maximum adsorption (mg/g). K_L is Langmuir adsorption equilibrium constant (1/mg), K_f is Freundlich constant (mg/g) $(L/mg)^{1/n}$. n is a constant which shows adsorption rate (Nasseh et al., 2019).

The fundamental properties of the Langmuir isotherm may be defined in terms of a dimensionless constant known as the separation factor or equilibrium parameter R_L, which is used to forecast whether the examined adsorption system is favorable or unfavorable. Eq. (5) was used to define it.

$$R_L R_L = \frac{1}{(1 + K_L C_0)} \tag{5}$$

Where C_0 is the initial RR198 concentration in (mg/L) and K_L is the Langmuir adsorption equilibrium constant in (L/mg). Unfavorable (RL greater than 1), linear (R_L = 1), favorable (0 < R_L less than 1), or irreversible (R_L = 0) adsorption is indicated by the value of R_L.

The Temkin isotherm (Fig. 8d) takes adsorbent-adsorbate relationships into account. The heat of adsorption of all molecules might fall linearly instead of logarithmically, according to this model, which ignores very low and high concentrations. Eqs. (6) and (7) show the linear formulation of Temkin isotherm (Al-Trawneh et al., 2021).

$$q_e = B_T lnK_T + B_T lnC_e \tag{6}$$

$$b_T = (RT)/(B_T) \tag{7}$$

The Temkin adsorption potential (L/g) is represented by the K_T, whereas the B_T and b_T are constants. The universal gas constant and the temperature, respectively, are R and T.

The adsorption isotherms profile shows the adsorption mechanism. As shown in the Table. 1, the value of R^2 is higher in the Freundlich isotherm, so RR 198 dye adsorption follows the Freundlich isotherm more, which uses a multilayer adsorption mechanism on the heterogeneous adsorbent surface. In the study by Lu et al., the mechanism of rhodamine B adsorption by the adsorbent follows the Freundlich isotherm model, which indicates the suitability of this isotherm model (Lu et al., 2019).

3.2.6. RR198 adsorption kinetic study

In the RR198 dye adsorption process, *pseudo*-first-order and *pseudo*-second-order kinetic models were surveyed. In adsorption kinetics studies, the rate of the adsorption process has been investigated, which is used to design, model, and operate processes in the reaction medium (Baghapour et al., 2014, Sanad et al., 2021a).

The *pseudo*-first-order kinetic (Eq. (6)) and *pseudo*-second-order kinetic (Eq. (7)) were calculated by the following formulas.

$$log(q_e - q_t) = log\ q_e - - K_1 t \tag{8}$$

q_t and q_e are the amount of adsorbate on the adsorbent (mg/g), t is the time of adsorption, K_1 is the *pseudo*-first-order adsorption rate constant (1/min). The graph of log $(q_e\text{-}q_t)$ versus t was used to determine the value of the constant K and R^2 coefficient (Nasseh et al., 2019).

$$\frac{t}{q_t} = \frac{1}{K_2 q_e^2} + \frac{1}{q_e} t \tag{9}$$

K_2 is *pseudo*-second-order adsorption rate constant (g/ (mg. min)). The graph of t/q_t versus t was used to determine the speed parameters. The slope and y-intercept of the diagram were used to calculate the values of q_e and K_2 (Nasseh et al., 2019).

If a straight line is obtained when plotting the molecules adsorbed versus the square root of the contact time,

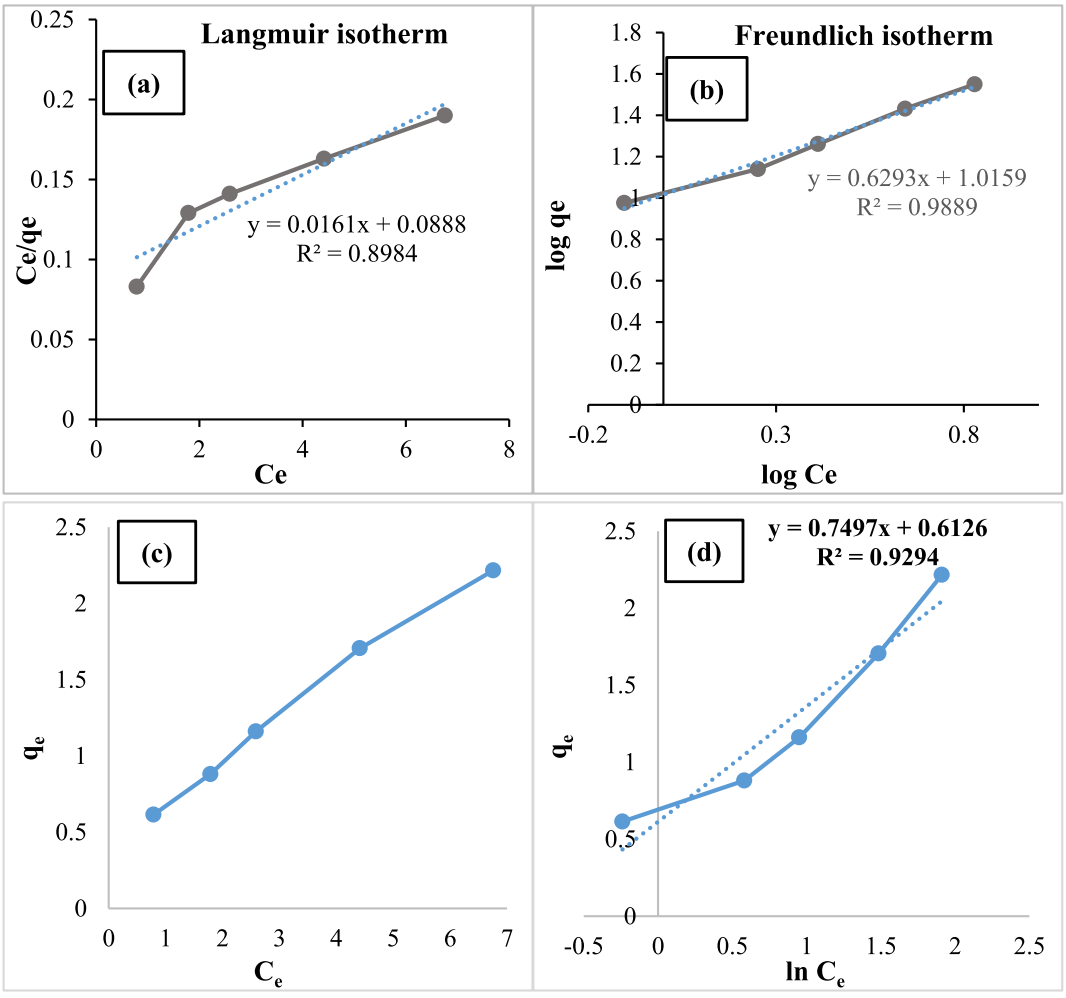

Fig. 8 The Langmuir isotherm (a), the Freundlich isotherm (b), q_e vs. C_e (c), and Temkin isotherm (d) for the RR198 adsorption under optimal conditions (pH: 3, RR198 concentration 10 mg/L, adsorbent dose: 1.5 g/L, and contact time: 10 min).

Table 1 The Langmuir, Freundlich, and Temkin isotherm parameters (pH: 3, adsorbent dose: 1.5 g/L, contact time: 10 min, and RR198 concentration: 10, 15, 20, 30, 40 mg/L).

Adsorbent	Freundlich isotherm			Langmuir isotherm				Temkin		
$CoFe_2O_4$@MC/AC	R^2	K_f [(mg/g) (1/mg)]	1/n	R^2	R_L	q_m (mg/g)	K_L (L/mg)	R^2	B_1	K_t (L/mg)
	0.989	10.351	0.629	0. 898	0.084 0.056 0.042 0.028 0.021	62.504	0.181	0.929	0.749	2.264

intraparticle diffusion is rate-limiting in the adsorption system. Weber and Morris (1963) gave the most extensively used intra-particle diffusion equation for adsorption systems (Ofomaja et al., 2020, Weber Jr and Morris, 1963):

$$q_t = k_i t^{0.5} + C \quad (10)$$

Where *ki* is intraparticle diffusion rate constant (g/mg.min) and the intercept of the plot, *C*, shows the boundary layer impact or surface adsorption, and it was discovered that the stronger the intercept, the higher the influence of surface adsorption in the rate-limiting phase. The curve can't pass

Table 2 The kinetic parameters (pH: 3, adsorbent dose: 1.5 g/L, and contact time: 10 min).

Adsorbent	*Pseudo*-first-order kinetic model			*Pseudo*-second-order kinetic model			Intraparticle kinetic model		
$CoFe_2O_4$@MC/AC	R^2	K_1 (1/min)	q_e (mg/g)	R^2	K_2 (g/mg.min)	q_e (mg/g)	R^2	K_P (mg/g. min^{-5})	C (mg/g)
	0.168	−0.084	0.045	0.995	0.151	2.579	0.935	2.397	0.264

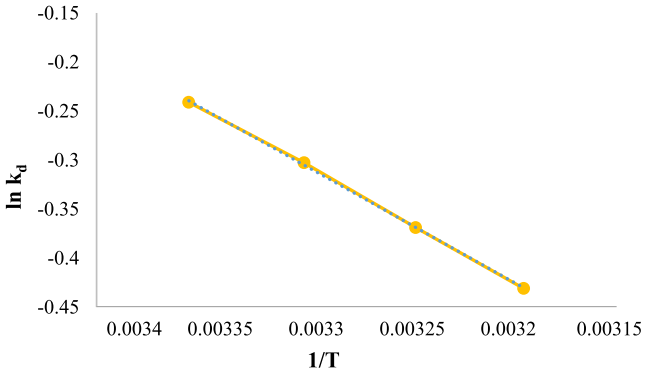

Fig. 9 The thermodynamic for the RR198 adsorption under optimal conditions (pH: 3, RR198 concentration 10 mg/L, adsorbent dose: 1.5 g/L, and contact time: 10 min).

through the origin when the kinetic analysis was conducted using the intraparticle diffusion model, showing that intraparticle diffusion was not the primary rate-limiting process.

According to Table 2, the value of R^2 in *pseudo*-second-order is greater than *pseudo*-first-order, then the adsorption process follows the *pseudo*-second-order kinetic more, as a result, the best model for the RR 198 adsorption process was *pseudo*-second-order kinetic, which had $R^2 = 0.995$ in the concentration of 10 mg/L. Baghapour et al. conducted a study on removing RR 198 by multiwall carbon nanotubes, they concluded that in concentrations of 50, 100, and 200 mg/L, the *pseudo*-second-order kinetic is the best model for the adsorption process with $R^2 = 0.995$ (Baghapour et al., 2014).

3.2.7. Thermodynamic evaluation of the RR198 adsorption process

In thermodynamic studies, the effect of 25, 30, 35, and 40 °C temperatures on the RR 198 dye adsorption process were studied. In this section, thermodynamic parameters that include ΔH, ΔS, and ΔG were investigated. The curve of thermodynamic for the RR198 adsorption was shown in Fig. 9. The Gibbs free energy changes (Eq. (8)), standard enthalpy, and standard entropy changes (Eq. (9)) were calculated by the following formulas.

Table 3 The thermodynamic parameters (pH: 3, adsorbent dose: 1.5 g/L, and contact time: 10 min).

T (k)	ΔG (kJ/mol)	ΔH (kJ/mol)	ΔS (J/mol.k)
298	−20.318	−9.862	35.086
303	−20.493		
308	−20.669		
313	−20.844		

$$\Delta G = -RT.lnk_d \tag{11}$$

$$lnK_d = \frac{\Delta s}{R} - \frac{\Delta H}{RT} \tag{12}$$

ΔG is Gibbs free energy changes, R is the universal gas constant equal to 8.314 J/mol/K, T is the temperature (K), K_d is the thermodynamic equilibrium constant, ΔS is the standard entropy (kJ/mol), ΔH is the standard enthalpy changes (kJ/mol).

Then, after calculating the thermodynamic equilibrium constant for Gibbs free energy and different temperatures, the graph of lnK_d versus 1/T was drawn and the values of ΔS and ΔH were determined using their slope and origin-intercept (Nasseh et al., 2019).

According to the result obtained in Table 3, the values of ΔS = 35.087, ΔH = -9.862 and ΔG = -20.318, where the positive ΔS indicates the willingness of the RR 198 to move spontaneously towards the adsorbent and the negative ΔH indicates the exothermic process, which means that with increasing temperature the rate of adsorption decreases. So, because the adsorption process' efficiency declines with increasing temperature, it's a type of physical adsorption. If the chemical adsorption process operated the other way around, it would be because chemical adsorption requires energy, which rises with temperature and energy efficiency. In general, physical and chemical adsorption is always present, but here physical adsorption takes priority due to rising temperatures and declining efficacy (Darwish et al., 2019, Bering et al., 1972). Finally, the ΔG parameter indicates that the adsorption process is spontaneous, here because this value is negative, the adsorption process is spontaneous. Lu et al. concluded that the adsorption process of RhB on the adsorbent surface is spontaneous and exothermic (Lu et al., 2019).

3.3. Comparison with other adsorbents

This adsorbent showed a very high performance in removing dye when compared to other adsorbents, while having a lower adsorbent dosage and a shorter processing time, indicating that it is economical and cost-effective (Table 4).

3.4. Investigation of recyclability and the chemical stability of $CoFe_2O_4$@MC/AC

Economically, the regeneration study of synthesized adsorbents is of great importance. The adsorption assessment of RR198 was done as described in the batch adsorption experiment. after using of adsorbent under the following condition (RR198concentration 10 mg/L, pH 3, contact time 10 min, nanocomposite dose 1.5 g/L, and temperature 25 °C), it was separated by a magnet and regenerated by NaOH 0.1 *N*, then

Table 4 Comparison of $CoFe_2O_4$@MC/AC with other adsorbents.

No.	Adsorbent	Pollutant	Dose of adsorbent	Dye concentration	Contact time	Efficiency (%)	Ref.
1	Walnut shell	Reactive Red 198	2 g/L	20 mg/L	40 min	87.17%	(Alimohammadi et al., 2016)
2	Pomegranate seeds	Reactive Red 198	2 g/L	25 mg/L	30 min	87.64%	(Ghaneian et al., 2015)
3	NH_2-MCM-41	Acid fuchsine	2 g/L	100 mg/L	240 min	92.54%	(Wu et al., 2014)
4	NH_2-MCM-41	Acid orange II	2 g/L	100 mg/L	240 min	95.64%	(Wu et al., 2014)
5	Manila Grass Activated Carbon	Novacron Brilliant Red EC-3GL	10 g/L	50 mg/L	90 min	85.52%	(Charnkeitkong and Phoophuangpairoj, 2020)
6	Chitosan/MgO	Reactive Blue 4	9.33 g/L	100 mg/L	120 min	77.62%	(Nga et al., 2020)
7	$CoFe_2O_4$@MC/AC	Reactive Red 198	1.5 g/L	10 mg/L	10 min	92.2 %	This work

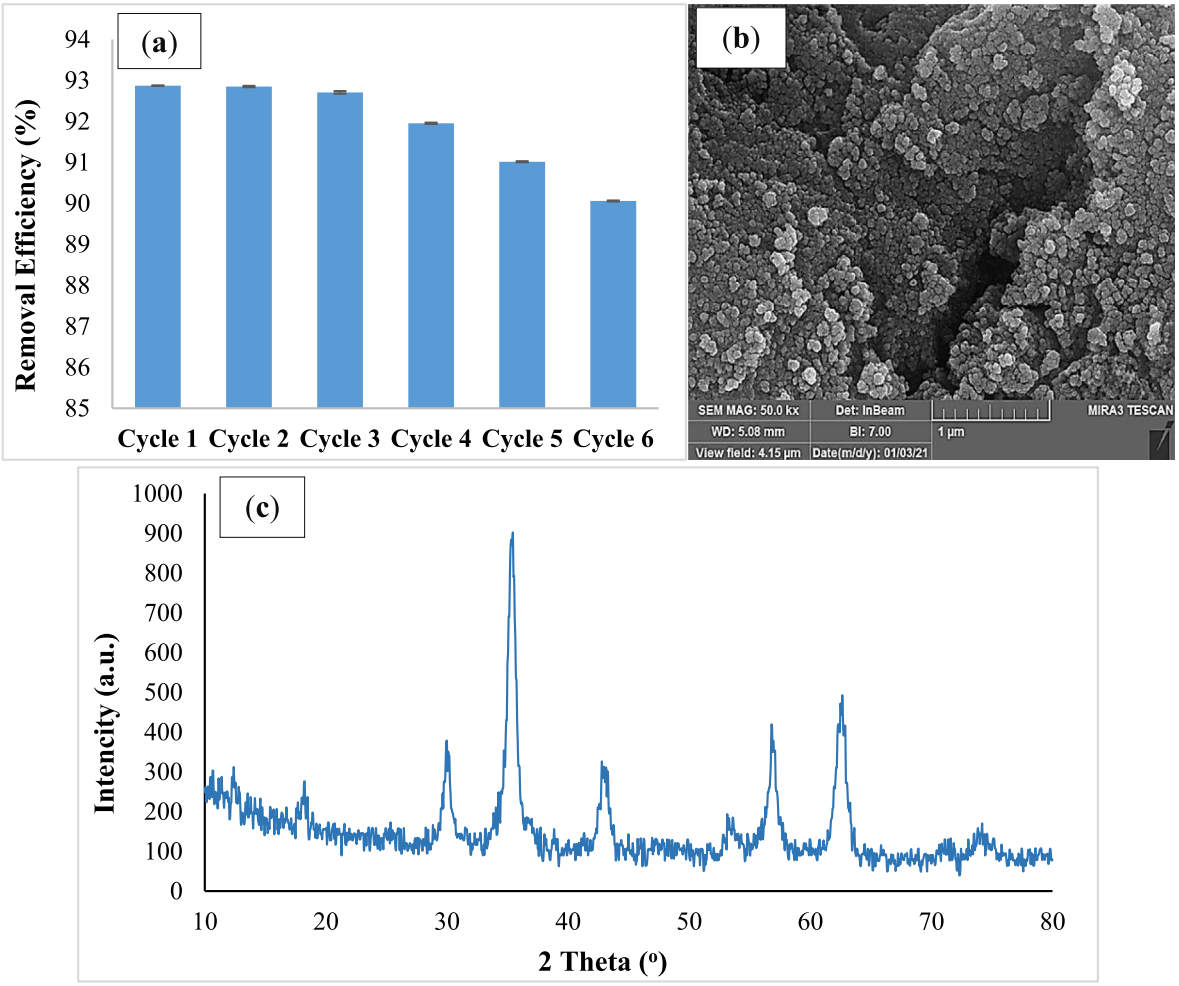

Fig. 10 Regeneration (a), FESEM image (b), and XRD (c) of magnetic nano-adsorbent after six recycling cycles.

it was washed several times by distilled water and dried in an oven at 70 °C. After the adsorbent dried, it was used again for the next cycle. For the determination of adsorbent reusability potential, the adsorption–desorption process was repeated up to six cycles in the optimum conditions. As shown in Fig. 10 a, after six cycles, the removal efficiency was reduced from 93% to 90.1% but the removal efficiency was almost retained after six cycles. This amount of reduction in dye adsorption efficiency can be due to the reduction of the adsorbent during washing and also the occupation of the adsorbent surface by the dye (Chu et al., 2015). The chemical resistance of the adsorbent was then assessed using XRD and FESEM procedures after the six cycles (Fig. 10 b, and c). The morphology of the adsorbent was determined to be preserved after the sixth cycle, according to FESEM data. The adsorbent's XRD pattern after the sixth cycle also revealed that the crystalline structure was still intact, and the strong peaks in the XRD analysis suggested that the adsorbent was chemically stable.

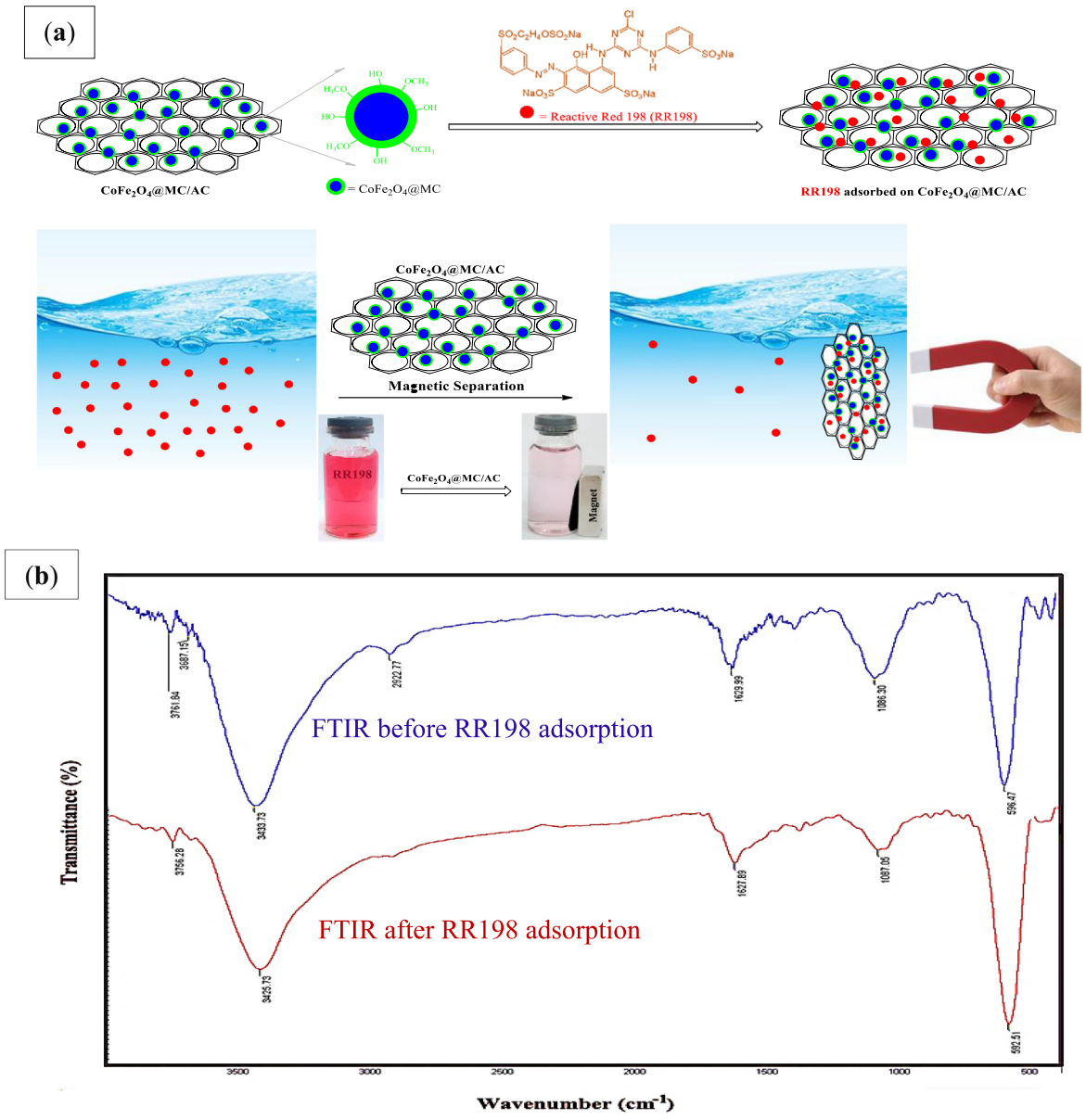

Fig. 11 FTIR of $CoFe_2O_4$@MC/AC before and after RR198 adsorption.

3.5. Adsorption mechanism and the role of methylcellulose

The adsorption mechanism of RR198 by $CoFe_2O_4$@MC/AC magnetic adsorbent was shown in Fig. 11 a, and comparative FTIR of $CoFe_2O_4$@MC/AC before and after Reactive Red 198 adsorption is demonstrated in Fig. 11 b.

However, due to the dye's surface binding, the FTIR spectra exhibit minor discrepancies. After RR198 sorption, the band at 3433 cm^{-1} for the O-H stretching vibration has shifted to a lower wavelength (3425 cm^{-1}), and the peak intensity has dropped. In addition, the stretching vibration C-O-C bond group at 1087 cm^{-1} shifts to 1066 cm^{-1}. Furthermore, the average intensity of the bands is lower in the $CoFe_2O_4$@-MC/AC. The hydroxyl and etheric groups on the surfaces of the $CoFe_2O_4$@MC/AC are implicated in the sequester of RR198, leading to the creation of inner-sphere surface complexes, based on these alterations and the findings of desorption investigations. Fig. 9 b depicts the various processes for the capture of RR198 by $CoFe_2O_4$@MC/AC discussed above.

In addition, the effectiveness of $CoFe_2O_4$@MC/AC and $CoFe_2O_4$/AC in terms of RR198 adsorption was assessed under optimal conditions (Fig. 12a). According to the findings, removal efficiencies of 92.2% and 72% were attained utilizing $CoFe_2O_4$@MC/AC and $CoFe_2O_4$/AC, respectively. After 10 min, $CoFe_2O_4$@MC/AC exhibited a considerably better removal efficiency than $CoFe_2O_4$/AC. Also, Fig. 12 b-c show FESEM pictures of $CoFe_2O_4$@MC/AC and $CoFe_2O_4$/AC, respectively. In the absence of MC, $CoFe_2O_4$/AC was produced. In comparison to the synthesized $CoFe_2O_4$@MC/AC, the $CoFe_2O_4$/AC sample does have more aggregated. By evaluating FESEM pictures, it can also be determined that $CoFe_2O_4$@MC/AC particles generated with MC aggregated much less than $CoFe_2O_4$/AC particles produced without MC. The

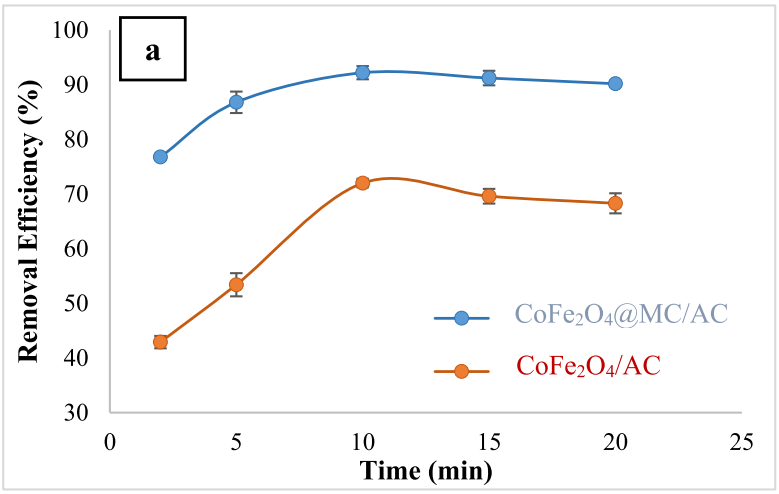

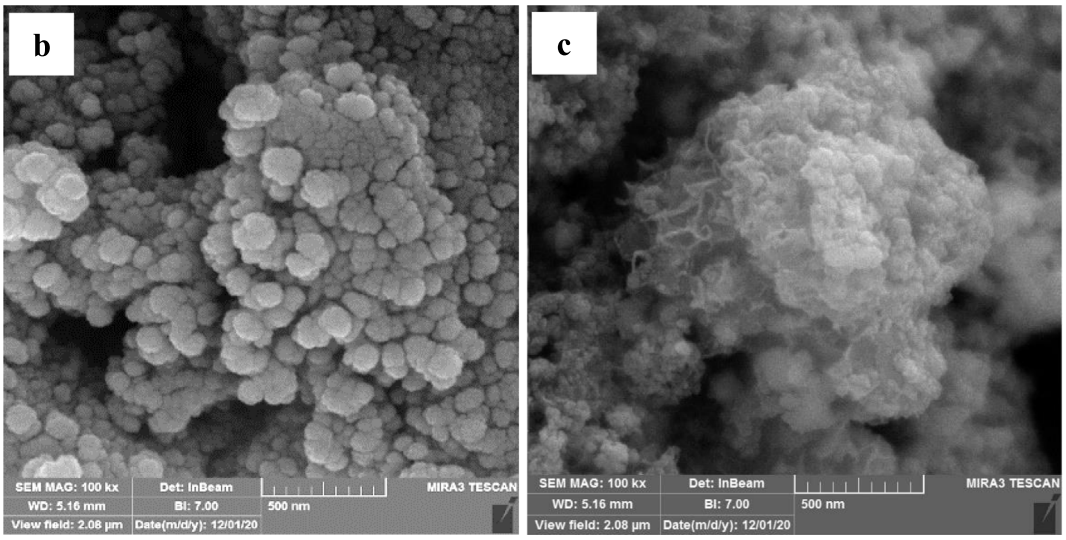

Fig. 12 The performance comparison of $CoFe_2O_4$@MC/AC and $CoFe_2O_4$/AC under optimal conditions for adsorption of RR198 (RR198 concentration = 10 mg/L, pH = 3, adsorbent dose = 1.5 g/L, and temperature = 25 °C) (a), FESEM images of $CoFe_2O_4$@MC/AC (b) and $CoFe_2O_4$/AC (c).

fact that $CoFe_2O_4$@MC/AC was templated from methylcellulose with methoxy groups explains this outcome. There are two possible explanations for this conclusion (Tamaddon et al., 2020). The presence of MC during the synthesis of $CoFe_2O_4$@MC/AC could be the first cause, as $CoFe_2O_4$@MC/AC has a greater surface area than $CoFe_2O_4$/AC. The surface area of the magnetic nano-adsorbent is increased, resulting in a greater surface area of adsorbent contacted to RR198 and higher RR198 adsorption efficiency. As well, electrostatic interaction between RR198 and $CoFe_2O_4$@MC/AC surface is also caused by methoxy and hydroxyl groups in MC. As a result, a higher number of RR198 molecules are put on the surface of the adsorbent, causing more contact and boosting the adsorption characteristics.

3.6. Investigation of process efficiency on real wastewater

To evaluate the efficiency of the process on real wastewater, the wastewater was first taken from the campus of Kerman University of Medical Sciences and its characteristics, including COD = 26.1 mg/L, BOD_5 = 8 mg/L, TSS = 78 mg/L, TDS = 1194 mg/L, TKN = 1.82 mg/L, Phosphate = 38.38 mg/L, Nitrate = 1.4 mg/L, Sulfate = 134.5 mg/L, and pH = 7.38 were determined. Then the wastewater conditions were optimized and dye removal efficiency was measured by the adsorbent. To evaluate the process on a real sample, 10 mg/l dye was spiked to the sample initially, and the sample conditions were adjusted to optimum on the synthetic sample. The sample is centrifuged after the operation to eliminate turbidity from the real wastewater and to determine the dye concentration in the sample. Under optimum condition (RR 198 concentration = 10 mg/L, adsorbent dose = 1.5 g/L, temperature = 25 °C, time = 10 min and pH = 3), the dye removal efficiency was 78%, which is relatively desirable. Due to the presence of cations, anions, TDS, and TSS in the real wastewater, the RR198 removal efficiency decreased.

4. Conclusion

The microwave method was used to synthesize $CoFe_2O_4$@MC/AC nano-adsorbent in the presence of MC. FESEM EDS-Mapping & Linescan, FTIR, XRD, BET, and VSM

analyses were used to characterize the structure. According to the findings, the particle size of this magnetic nanocomposite is around 11 nm, it is produced evenly and quasi-spherically, and the element distribution at the nanoparticle surface is uniform. The nanoparticle had a specific surface area of 128.22 m^2/g and saturation magnetization (Ms) of 57.91 emu/g, allowing it to be separated from the reaction media using an external magnet. The crystal structure of nanoparticles is still retained after composite with activated carbon, according to XRD analysis. According to the results, the maximum removal efficiency of RR198 under optimal conditions (RR198 concentration 10 mg/L, pH 3, the dose of adsorbent 1.5 g/L, and temperature 25 °C) in synthetic and real wastewater samples were 92.2% and 78%, respectively. The dye adsorption process in this adsorbent follows the Freundlich isotherm, *pseudo*-second-order kinetic. In terms of the thermodynamic negative values of Gibbs free energy, ΔH = -9.8621 (kJ/mol), and ΔS = 35.0867 (J/mol.k), this process is exothermic that decreases the dye removal efficiency with increasing temperature. The result of recovery and reusability of this adsorbent showed that this adsorbent after 6 cycles of use and recovery, still has a removal efficiency of about 90.1%, which is an acceptable amount.

Declaration of Competing Interest

The authors declare that they have no known competing financial interests or personal relationships that could have appeared to influence the work reported in this paper.

Acknowledgments

This research with project number 98001206 and IR.KMU.REC.1399.280 ethic approval cod was conducted in the Student Research Committee of Kerman University of Medical Sciences. This research was supported by the Vice-Chancellor for Research and Technology of Kerman University of Medical Sciences.

References

Afolabi, H.K., Nasef, M.M., Nordin, N.A.H.M., Ting, T.M., Harun, N.Y., Saeed, A.A.H., 2021. Isotherms, kinetics, and thermodynamics of boron adsorption on fibrous polymeric chelator containing glycidol moiety optimized with response surface method. Arabian J. Chem. 14, 103453.

Aichour, A., Zaghouane-Boudiaf, H., Djafer Khodja, H. 2022. Highly removal of anionic dye from aqueous medium using a promising biochar derived from date palm petioles: Characterization, adsorption properties and reuse studies. Arab. J. Chem. 15, 103542.

Al-Trawneh, S.A., Jiries, A.G., Alshahateet, S.F., Sagadevan, S., 2021. Phenol removal from aqueous solution using synthetic V-shaped organic adsorbent: Kinetics, isotherm, and thermodynamics studies. Chem. Phys. Lett. 781, 138959.

Alimohammadi, Z., Younesi, H., Bahramifar, N., 2016. Batch and column adsorption of reactive red 198 from textile industry effluent by microporous activated carbon developed from walnut shells. Waste Biomass Valorization 7, 1255–1270.

Baghapour, M.A., Pourfadakari, S., Mahvi, A.H., 2014. Investigation of Reactive Red Dye 198 removal using multiwall carbon nanotubes in aqueous solution. J. Ind. Eng. Chem. 20, 2921–2926.

Bering, B., Dubinin, M., Serpinsky, V., 1972. On thermodynamics of adsorption in micropores. J. Colloid Interface Sci. 38, 185–194.

Bhowmik, M., Kanmani, M., Debnath, A., Saha, B., 2019. Sono-assisted rapid adsorption of anionic dye onto magnetic CaFe2O4/MnFe2O4 nanocomposite from aqua matrix. Powder Technol. 354, 496–504.

BRABERS, V. 1969. Infrared spectra of cubic and tetragonal manganese ferrites. Phys. Status Solidi *(b)*, 33, 563–572.

Carneiro, P.A., Umbuzeiro, G.A., Oliveira, D.P., Zanoni, M.V.B., 2010. Assessment of water contamination caused by a mutagenic textile effluent/dyehouse effluent bearing disperse dyes. J. Hazard. Mater. 174, 694–699.

Chang, S., Zhang, Q., Lu, Y., Wu, S., Wang, W., 2020. High-efficiency and selective adsorption of organic pollutants by magnetic CoFe2O4/graphene oxide adsorbents: Experimental and molecular dynamics simulation study. Sep. Purif. Technol. 238, 116400.

Charnkeitkong, P., Phoophuangpairoj, R. Modification of Manila Grass Activated Carbon for Reactive Dye Adsorption from Textile Printing Wastewater. IOP Conference Series: Materials Science and Engineering, 2020. IOP Publishing, 012043.

Chavoshani, A., Amin, M. M., Asgari, G., Seidmohammadi, A., Hashemi, M. 2018. Microwave/hydrogen peroxide processes. *Advanced Oxidation Processes for Waste Water Treatment*. Elsevier.

Chu, L., Liu, C., Zhou, G., Xu, R., Tang, Y., Zeng, Z., Luo, S., 2015. A double network gel as low cost and easy recycle adsorbent: highly efficient removal of Cd (II) and Pb (II) pollutants from wastewater. J. Hazard. Mater. 300, 153–160.

Crini, G. 2005. Recent developments in polysaccharide-based materials used as adsorbents in wastewater treatment. *Progress in polymer science*, 30, 38–70.

Crini, G., 2006. Non-conventional low-cost adsorbents for dye removal: a review. Bioresour. Technol. 97, 1061–1085.

Darwish, A., Rashad, M., Al-Aoh, H.A., 2019. Methyl orange adsorption comparison on nanoparticles: Isotherm, kinetics, and thermodynamic studies. Dyes Pigm. 160, 563–571.

Das, P., Debnath, A., 2021. Reactive orange 12 dye adsorption onto magnetically separable CaFe2O4 nanoparticles synthesized by simple chemical route: kinetic, isotherm and neural network modeling. Water Pract. Technol. 16, 1141–1158.

Das, P., Debnath, A., Saha, B., 2020a. Ultrasound-assisted enhanced and rapid uptake of anionic dyes from the binary system onto MnFe2O4/polyaniline nanocomposite at neutral pH. Appl. Organomet. Chem. 34, e5711.

Das, P., Debnath, P., Debnath, A., 2021. Enhanced sono-assisted adsorptive uptake of malachite green dye onto magnesium ferrite nanoparticles: kinetic, isotherm and cost analysis. Environ. Nanotechnol. Monit. Manage. 16, 100506.

Das, P., Nisa, S., Debnath, A., Saha, B., 2020b. Enhanced adsorptive removal of toxic anionic dye by novel magnetic polymeric nanocomposite: optimization of process parameters. J. Dispersion Sci. Technol., 1–16

Datta, D., Kerkez Kuyumcu, Ö., Bayazit, Ş.S., Abdel Salam, M., 2017. Adsorptive removal of malachite green and Rhodamine B dyes on Fe_3O_4/activated carbon composite. J. Dispers. Sci. Technol. 38, 1556–1562.

Debnath, A., Bera, A., Chattopadhyay, K., Saha, B., 2017. Facile additive-free synthesis of hematite nanoparticles for enhanced adsorption of hexavalent chromium from aqueous media: Kinetic, isotherm, and thermodynamic study. Inorg. Nano-Metal Chem. 47, 1605–1613.

Debnath, B., Majumdar, M., Bhowmik, M., Bhowmik, K.L., Debnath, A., Roy, D.N., 2020. The effective adsorption of tetracycline onto zirconia nanoparticles synthesized by novel microbial green technology. J. Environ. Manage. 261, 110235.

Dehghani, M.H., Pourshabanian, M., Heidarinejad, Z., 2018. Experimental data on the adsorption of Reactive Red 198 from aqueous solution using Fe3O4 nanoparticles: Optimization by response surface methodology with central composite design. Data in brief 19, 2126–2132.

Fadaei, S., Moghadam, F.N., Hashemi, M., Pourzamani, H., 2017. BTEX removal from aqueous solution by modified multi-walled carbon nanotubes with ozone. Anuario do Instituto de Geociencias 40, 235–242.

Fahad, M., Gilbert, M., Dickens, P., 2017. Microscopy and FTIR investigations of the thermal gelation of methylcellulose in glycols. Polymer Science, Series A 59, 88–97.

Gerard, N., Krishnan, R.S., Ponnusamy, S.K., Cabana, H., Vaidyanathan, V.K., 2016. Adsorptive potential of dispersible chitosan coated iron-oxide nanocomposites toward the elimination of arsenic from aqueous solution. Process Saf. Environ. Prot. 104, 185–195.

Ghaneian, M., Jamshidi, B., Dehvari, M., Amrollahi, M., 2015. Pomegranate seed powder as a new biosorbent of reactive red 198 dye from aqueous solutions: adsorption equilibrium and kinetic studies. Res. Chem. Intermed. 41, 3223–3234.

Gupta, V.K., Ali, I., Saleh, T.A., Nayak, A., Agarwal, S., 2012. Chemical treatment technologies for waste-water recycling—an overview. RSC Adv. 2, 6380–6388.

Haffad, H., Zbair, M., Anfar, Z., Ahsaine, H.A., Bouhlal, H., Khallok, H., 2019. Removal of reactive red-198 dye using chitosan as an adsorbent: optimization by central composite design coupled with response surface methodology. Toxin Rev.

Hashemi, M., Amin, M.M., Sadeghi, S., Menglizadeh, N., Mohammadi, F., Patastar, S., Chavoshani, A., Rezaei, S., 2017. Coupling adsorption by NiO nanopowder with UV/H2O2 process for Cr (VI) removal. J. Adv. Environm. Health Res. 5, 210–219.

Iervolino, G., Vaiano, V., Palma, V., 2019. Enhanced removal of water pollutants by dielectric barrier discharge non-thermal plasma reactor. Sep. Purif. Technol. 215, 155–162.

Javid, N., Nasiri, A., Malakootian, M., 2019. Removal of nonylphenol from aqueous solutions using carbonized date pits modified with ZnO nanoparticles. Desalination Water Treatm. 141, 140–148.

Kamranifar, M., Khodadadi, M., Samiei, V., Dehdashti, B., Sepehr, M.N., Rafati, L., Nasseh, N., 2018. Comparison the removal of reactive red 195 dye using powder and ash of barberry stem as a low cost adsorbent from aqueous solutions: Isotherm and kinetic study. J. Mol. Liq. 255, 572–577.

Kausar, A., Iqbal, M., Javed, A., Aftab, K., Bhatti, H.N., Nouren, S., 2018. Dyes adsorption using clay and modified clay: A review. J. Mol. Liq. 256, 395–407.

Li, J., Jiang, B., Liu, Y., Qiu, C., Hu, J., Qian, G., Guo, W., Ngo, H. H., 2017. Preparation and adsorption properties of magnetic chitosan composite adsorbent for Cu2 + removal. J. Cleaner Prod. 158, 51–58.

Liang, Y.-D., He, Y.-J., Wang, T.-T., Lei, L.-H., 2019. Adsorptive removal of gentian violet from aqueous solution using CoFe2O4/activated carbon magnetic composite. J. Water Process Eng. 27, 77–88.

Liebeck, B.M., Hidalgo, N., Roth, G., Popescu, C., Böker, A., 2017. Synthesis and characterization of methyl cellulose/keratin hydrolysate composite membranes. Polymers 9, 91.

Lu, H., Li, Y., Wang, Y., Li, X., 2019. Preparation of CoFe2O4@vacancy@ mSiO2 core-shell composites for removal of organic pollutant in aqueous solution. J. Saudi Chem. Soc. 23, 536–545.

Mahdizadeh, H., Nasiri, A., Gharaghani, M.A., Yazdanpanah, G., 2020. Hybrid UV/COP advanced oxidation process using ZnO as a catalyst immobilized on a stone surface for degradation of acid red 18 dye. MethodsX 7, 101118.

Mahmoud, M., Ismail, A.A., Sanad, M., 2012. Developing a cost-effective synthesis of active iron oxide doped titania photocatalysts loaded with palladium, platinum or silver nanoparticles. Chem. Eng. J. 187, 96–103.

Malakootian, M., Askarpuor, A., Amirmahani, N., Nasiri, Z., Nasiri, A., 2015. Removal of Hexavalent Chromium from Aqueous Solutions Using Magnetic Nanoparticles Coated with Alumina and Modified by Cetyl Trimethyl Ammonium Bromide. J. Commun. Health Res. 4, 177–193.

Malakootian, M., Hashemi, M., Toolabi, A., Nasiri, A., 2018a. Investigation of nickel removal using poly (amidoamine) generation 4 dendrimer (PAMAM G4) from aqueous solutions. J. Eng. Res. 6.

Malakootian, M., Kannan, K., Gharaghani, M.A., Dehdarirad, A., Nasiri, A., Shahamat, Y.D., Mahdizadeh, H., 2019a. Removal of metronidazole from wastewater by Fe/charcoal micro electrolysis fluidized bed reactor. J. Environ. Chem. Eng. 7, 103457.

Malakootian, M., Mahdizadeh, H., Khavari, M., Nasiri, A., Gharaghani, M.A., Khatami, M., Sahle-Demessie, E., Varma, R. S., 2020a. Efficiency of novel Fe/charcoal/ultrasonic micro-electrolysis strategy in the removal of Acid Red 18 from aqueous solutions. J. Environ. Chem. Eng. 8, 103553.

Malakootian, M., Nasiri, A., Alibeigi, A.N., Mahdizadeh, H., Gharaghani, M.A., 2019b. Synthesis and stabilization of ZnO nanoparticles on a glass plate to study the removal efficiency of acid red 18 by hybrid advanced oxidation process (Ultraviolet/ZnO/ultrasonic). Desalin. Water Treat 170, 325–336.

Malakootian, M., Nasiri, A., Heidari, M.R., 2020b. Removal of phenol from steel plant wastewater in three dimensional electrochemical (TDE) process using CoFe2O4@ AC/H2O2. Z. Phys. Chem. 234, 1661–1679.

Malakootian, M., Nasiri, A., Khatami, M., Mahdizadeh, H., Karimi, P., Ahmadian, M., Asadzadeh, N., Heidari, M.R., 2019c. Experimental data on the removal of phenol by electro-H2O2 in presence of UV with response surface methodology. MethodsX 6, 1188–1193.

Malakootian, M., Nasiri, A., Mahdizadeh, H., 2018b. Preparation of CoFe2O4/activated carbon@ chitosan as a new magnetic nanobiocomposite for adsorption of ciprofloxacin in aqueous solutions. Water Sci. Technol. 78, 2158–2170.

Malakootian, M., Smith, J., Gharaghani, M., Mahdizadeh, H., Nasiri, A., Yazdanpanah, G., 2020c. Decoloration of textile Acid Red 18 dye by hybrid UV/COP advanced oxidation process using ZnO as a catalyst immobilized on a stone surface. Desalin. Water Treat 182, 385–394.

Mehdinejad, M.H., Mengelizadeh, N., Bay, A., Pourzamani, H., Hajizadeh, Y., Niknam, N., Moradi, A.H., Hashemi, M., Mohammadi, H., 2018. Adsorption of methylene blue from aqueous solutions by cellulose and nanofiber cellulose and its electrochemical regeneration. Desalin. Water Treat. 110, 250–263.

Mittal, H., Ray, S.S., Okamoto, M., 2016. Recent progress on the design and applications of polysaccharide-based graft copolymer hydrogels as adsorbents for wastewater purification. Macromol. Mater. Eng. 301, 496–522.

Modi, K., Chhantbar, M., Joshi, H., 2006. Study of elastic behaviour of magnesium ferri aluminates. Ceram. Int. 32, 111–114.

Mohammadi, F., Yavari, Z., Rahimi, S., Hashemi, M., 2019. Artificial neural network modeling of Cr (VI) biosorption from aqueous solutions. J. Water Chem. Technol. 41, 219–227.

Moon, R.J., Martini, A., Nairn, J., Simonsen, J., Youngblood, J., 2011. Cellulose nanomaterials review: structure, properties and nanocomposites. Chem. Soc. Rev. 40, 3941–3994.

Moussavi, G., Mahmoudi, M., 2009. Removal of azo and anthraquinone reactive dyes from industrial wastewaters using MgO nanoparticles. J. Hazard. Mater. 168, 806–812.

Nasiri, A., Malakootian, M., Heidari, M.R., Asadzadeh, S.N., 2021a. CoFe2O4@Methylcelloluse as a New Magnetic Nano Biocomposite for Sonocatalytic Degradation of Reactive Blue 19. J. Polym. Environ. 29, 2660–2675.

Nasiri, A., Malakootian, M., Heidari, M.R., Asadzadeh, S.N., 2021b. CoFe 2 O 4@ Methylcelloluse as a New Magnetic Nano Biocomposite for Sonocatalytic Degradation of Reactive Blue 19. J. Polym. Environ., 1–16

Nasiri, A., Tamaddon, F., Mosslemin, M, H., Amiri Gharaghani, M., Asadipour, A. 2019a. Magnetic nano-biocomposite CuFe2O4@methylcellulose (MC) prepared as a new nano-photo-

catalyst for degradation of ciprofloxacin from aqueous solution. Environm. Health Eng. Managem. J. 6, 41–51.
Nasiri, A., Tamaddon, F., Mosslemin, M.H., Faraji, M., 2019b. A microwave assisted method to synthesize nanoCoFe2O4@ methyl cellulose as a novel metal-organic framework for antibiotic degradation. MethodsX 6, 1557–1563.
Nasiri, A., Tamaddon, F., Mosslemin, M.H., Faraji, M., 2019c. A microwave assisted method to synthesize nanoCoFe2O4@methyl cellulose as a novel metal-organic framework for antibiotic degradation. MethodsX 6, 1557–1563.
Nasiri, A., Tamaddon, F., Mosslemin, M.H., Gharaghani, M.A., Asadipour, A., 2019d. New magnetic nanobiocomposite CoFe 2 O 4@ methycellulose: facile synthesis, characterization, and photocatalytic degradation of metronidazole. J. Mater. Sci.: Mater. Electron. 30, 8595–8610.
Nasseh, N., Barikbin, B., Taghavi, L., Nasseri, M.A., 2019. Adsorption of metronidazole antibiotic using a new magnetic nanocomposite from simulated wastewater (isotherm, kinetic and thermodynamic studies). Compos. B Eng. 159, 146–156.
Nga, N.K., Chau, N.T.T., Viet, P.H., 2020. Preparation and characterization of a chitosan/MgO composite for the effective removal of reactive blue 19 dye from aqueous solution. J. Sci.: Adv. Mater. Devices.
Ofomaja, A.E., Naidoo, E.B., Pholosi, A., 2020. Intraparticle diffusion of Cr (VI) through biomass and magnetite coated biomass: A comparative kinetic and diffusion study. S. Afr. J. Chem. Eng. 32, 39–55.
Pourzamani, H., Hashemi, M., Bina, B., Rashidi, A., Amin, M.M., Parastar, S., 2018. Toluene removal from aqueous solutions using single-wall carbon nanotube and magnetic nanoparticle–hybrid adsorbent. J. Environ. Eng. 144, 04017104.
Pourzamani, H., Parastar, S., Hashemi, M., 2017. The elimination of xylene from aqueous solutions using single wall carbon nanotube and magnetic nanoparticle hybrid adsorbent. Process Saf. Environ. Prot. 109, 688–696.
Pradeep, A., Priyadharsini, P., Chandrasekaran, G., 2008. Sol–gel route of synthesis of nanoparticles of MgFe2O4 and XRD, FTIR and VSM study. J. Magn. Magn. Mater. 320, 2774–2779.
Qiu, W., Yang, D., Xu, J., Hong, B., Jin, H., Jin, D., Peng, X., Li, J., Ge, H., Wang, X., 2016. Efficient removal of Cr (VI) by magnetically separable CoFe2O4/activated carbon composite. J. Alloy. Compd. 678, 179–184.
Rajabi, S., Nasiri, A., Hashemi, M., 2022. Enhanced activation of persulfate by CuCoFe2O4@ MC/AC as a novel nanomagnetic heterogeneous catalyst with ultrasonic for metronidazole degradation. Chemosphere 286, 131872.
Rashad, M., Ibrahim, A., Rayan, D., Sanad, M., Helmy, I. 2017a. Environmental Nanotechnology, Monitoring & Management.
Rashad, M., Ibrahim, A., Rayan, D., Sanad, M., Helmy, I., 2017b. Photo-Fenton-like degradation of Rhodamine B dye from waste water using iron molybdate catalyst under visible light irradiation. Environ. Nanotechnol. Monit. Manage. 8, 175–186.
Rogers, T.L., Wallick, D., 2012. Reviewing the use of ethylcellulose, methylcellulose and hypromellose in microencapsulation. Part 3: Applications for microcapsules. Drug Dev. Ind. Pharm. 38, 521–539.
Sadeghi, S., Raki, G., Amini, A., Mengelizadeh, N., Amin, M.M., Hashemi, M., 2018. Study of the effectiveness of the third generation polyamideamine and polypropylene imine dendrimers in removal of reactive blue 19 dye from aqueous solutions. Environm. Health Eng. Managem. J. 5, 197–203.
Salimi, F., Eskandari, M., Karami, C., 2017. Investigation of methylene blue adsorption in wastewater using nano-zeolite modified with copper. Desalin. Water Treatm. 85, 206–214.
Salimi, F., Rahimi, H., Karami, C., 2019a. Removal of methylene blue from water solution by modified nanogoethite by Cu. Desalin. Water Treat. 137, 334–344.
Salimi, F., Salimi, J., Golmohammadi, F., 2019b. Review on Applications of Adsorbents to Remove Phenolic Compounds from Wastewater. J. Water Wastewater Sci. Eng. 4, 16–33.
Sanad, M., Farahat, M., Khalek, M.A., 2021a. One-step processing of low-cost and superb natural magnetic adsorbent: kinetics and thermodynamics investigation for dye removal from textile wastewater. Adv. Powder Technol. 32, 1573–1583.
Sanad, M.M., Farahat, M.M., El-Hout, S.I., El-Sheikh, S.M., 2021b. Preparation and characterization of magnetic photocatalyst from the banded iron formation for effective photodegradation of methylene blue under UV and visible illumination. J. Environ. Chem. Eng. 9, 105127.
Sanjid Qais, D., Nazrul Islam, M., Hafiz Dzarfan Othman, M., Ekramul Mahmud, H. N. M., Emran Quayum, M., Anwarul Islam, M., Mohammad Ibrahim Ismail, I., Habib, A. 2021. Synthesis and characterization of nano-zinc oxide: adsorption of acid blue 92 dye, isotherms, thermodynamics and kinetics. Arab. J. Chem. 103627.
Santhosh, C., Daneshvar, E., Kollu, P., Peräniemi, S., Grace, A.N., Bhatnagar, A., 2017. Magnetic SiO2@ CoFe2O4 nanoparticles decorated on graphene oxide as efficient adsorbents for the removal of anionic pollutants from water. Chem. Eng. J. 322, 472–487.
Sobhanardakani, S., Ghoochian, M., Jameh-Bozorghi, S., Zandipak, R., 2017. Assessing of removal efficiency of Indigo carmine from wastewater using MWCNTs. Iranian J. Sci. Technol. Trans. A: Sci. 41, 1047–1053.
Sobhanardakani, S., Zandipak, R., 2015. Removal of anionic dyes (direct blue 106 and acid green 25) from aqueous solutions using Oxidized Multi-Walled Carbon Nanotubes. Iranian J. Health Sci. 3, 48–57.
Sobhanardakani, S., Zandipak, R., Khoshsafar, H., Zandipak, R., 2016. Removal of cationic dyes from aqueous solutions using NiFe2O4 nanoparticles. J. Water Supply Res. Technol. AQUA 65, 64–74.
Sobhanardakani, S., Zandipak, R., Sahraei, R., 2013. Removal of Janus Green dye from aqueous solutions using oxidized multi-walled carbon nanotubes. Toxicol. Environ. Chem. 95, 909–918.
Sun, X., Chen, F., Wei, J., Zhang, F., Pang, S., 2016. Preparation of magnetic triethylene tetramine-graphene oxide ternary nanocomposite and application for Cr (VI) removal. J. Taiwan Inst. Chem. Eng. 66, 328–335.
Sun, X., Yang, L., Li, Q., Zhao, J., Li, X., Wang, X., Liu, H., 2014. Amino-functionalized magnetic cellulose nanocomposite as adsorbent for removal of Cr (VI): synthesis and adsorption studies. Chem. Eng. J. 241, 175–183.
Tamaddon, F., Mosslemin, M.H., Asadipour, A., Gharaghani, M.A., Nasiri, A., 2020. Microwave-assisted preparation of ZnFe2O4@-methyl cellulose as a new nano-biomagnetic photocatalyst for photodegradation of metronidazole. Int. J. Biol. Macromol. 154, 1036–1049.
Torkian, L., Ashtiani, B.G., Amereh, E., Mohammadi, N., 2012. Adsorption of Congo red onto mesoporous carbon material: equilibrium and kinetic studies. Desalin. Water Treat. 44, 118–127.
Unnikrishnan, S., Khan, M.H., Ramalingam, K., 2018. Dye-tolerant marine Acinetobacter baumannii-mediated biodegradation of reactive red. Water Sci. Eng. 11, 265–275.
Weber JR, W. J. & Morris, J. C. 1963. Closure to "Kinetics of Adsorption on Carbon from Solution". J. Sanitary Eng. Divis. 89, 53–55.
Wu, Y., Zhang, M., Zhao, H., Yang, S., Arkin, A., 2014. Functionalized mesoporous silica material and anionic dye adsorption: MCM-41 incorporated with amine groups for competitive adsorption of Acid Fuchsine and Acid Orange II. RSC Adv. 4, 61256–61267.
Xu, J., Xin, P., Han, Y., Wang, P., Jin, H., Jin, D., Peng, X., Hong, B., Li, J., Ge, H., 2014. Magnetic response and adsorptive properties for methylene blue of CoFe2O4/CoxFey/activated carbon magnetic composites. J. Alloy. Compd. 617, 622–626.

Zandipak, R., Sobhanardakani, S., 2016. Synthesis of NiFe2O4 nanoparticles for removal of anionic dyes from aqueous solution. Desalin. Water Treat. 57, 11348–11360.

Zhang, J., Xie, Q., Wang, Y., Liu, J., Yao, X. The preparation and environmental applications of magnetic activated carbon. 2011 International Conference on Electrical and Control Engineering, 2011. IEEE, 1831–1834.

Zhang, Y., Yan, T., Yan, L., Guo, X., Cui, L., Wei, Q., Du, B., 2014. Preparation of novel cobalt ferrite/chitosan grafted with graphene composite as effective adsorbents for mercury ions. J. Mol. Liq. 198, 381–387.

Zhou, L., Ji, L., Ma, P.-C., Shao, Y., Zhang, H., Gao, W., Li, Y., 2014. Development of carbon nanotubes/CoFe2O4 magnetic hybrid material for removal of tetrabromobisphenol A and Pb (II). J. Hazard. Mater. 265, 104–114.